AD-766 143

RESEARCH ON THE PROPERTIES OF AMORPHOUS SEMICONDUCTORS AT HIGH TEMPERATURES

John P. deNeufville

Energy Conversion Devices, Incorporated
Troy, Michigan

17 June 1973

FIFTH SEMI-ANNUAL TECHNICAL REPORT

Contract DAHC15-70-C-0187

RESEARCH ON THE PROPERTIES OF AMORPHOUS SEMICONDUCTORS AT HIGH TEMPERATURES

Prepared by: Energy Conversion Devices, Inc.
1675 W. Maple Road
Troy, Michigan 48084

For: Advanced Research Projects Agency
[Order No. 1570; Program Code 0D10]

Contract Period: 18 May 1970 to 17 May 1973

Total Contract Price: $976,786.00

J. P. deNeufville
Program Technical Manager
313-549-7300

Copy No. 10

R71

Unclassified

Security Classification

DOCUMENT CONTROL DATA - R&D

(Security classification of title, body of abstract and indexing annotation must be entered when the overall report is classified)

1 ORIGINATING ACTIVITY (Corporate author)

Energy Conversion Devices, Inc.
1675 W. Maple Road, Troy, Michigan 48084

2a REPORT SECURITY CLASSIFICATION: Unclassified

2b GROUP: N/A

3 REPORT TITLE

RESEARCH ON THE PROPERTIES OF AMORPHOUS SEMICONDUCTORS AT HIGH TEMPERATURES

4 DESCRIPTIVE NOTES (Type of report and inclusive dates)

Fifth Semi-Annual Technical Report - 19 May 1970 to 18 May 1973

5 AUTHOR(S) (Last name, first name, initial)

deNeufville, John P.

6 REPORT DATE	7a TOTAL NO. OF PAGES	7b NO. OF REFS
17 June 1973	~~107~~ 71	49

8a CONTRACT OR GRANT NO.	9a ORIGINATOR'S REPORT NUMBER(S)
DAHC15-70-C-0187	516-5
b PROJECT NO. 1001/36	
c.	9b OTHER REPORT NO(S) (Any other numbers that may be assigned this report): None
d.	

10 AVAILABILITY/LIMITATION NOTICES

The distribution of this report is unlimited

11 SUPPLEMENTARY NOTES	12 SPONSORING MILITARY ACTIVITY
Details of illustrations in this document may be better studied on microfiche.	Advanced Research Projects Agency Arlington, Virginia 22209

13 ABSTRACT

1. Slowly evaporated amorphous films of As_2S_3 and As_2Se_3 undergo structural transformations when exposed to band gap illumination (photostructural transformation) or when annealed at ~ T_g (thermostructural transformation).

2. The initial structures of these evaporated amorphous solids appear to retain the molecularity which characterizes the vapor from which they are condensed.

3. In the case of slowly evaporated As_2S_3, the X-ray diffraction pattern is well characterized in terms of a dense-random packing of As_4S_6 molecular "hard-spheres", and the density calculated from this structural model agrees well with the measured density.

4. X-ray patterns of the transformed evaporated As_2S_3 and As_2Se_3 films closely resemble patterns of the sputtered films and the bulk glasses, indicating that polymerization of the molecular units occurs during the photostructural and thermostructural transformations of the evaporated films.

5. The refractive indices of the evaporated films increase irreversibly with annealing at T_g or with band-gap illumination, attaining values close to the bulk glass value for As_2S_3. No measurable change ($\Delta n < 0.01$) of refractive index accompanies illumination of the annealed films or annealing of the illuminated films.

(continued...)

DD FORM 1 JAN 64 1473

Unclassified

Security Classification

14. KEY WORDS	LINK A		LINK B		LINK C	
	ROLE	WT	ROLE	WT	ROLE	WT
Amorphous Semiconductors Amorphous Materials Chalcogenide Materials High Temperature Device Materials						

6. The optical absorption edge energy of the evaporated films decreases irreversibly with annealing at T_g or with band-gap illumination. A decrease of absorption edge energy accompanies exposure of the annealed films, and the edge can be reversibly restored by reannealing. This shift, termed photodarkening, is small for As_2Se_3 (~ 0.01 eV) and somewhat larger for As_2S_3 (~0.03 eV).

7. The irreversible optical effects accompany the irreversible structural effects, and can be qualitatively associated with polymerization, by analogy with the optical properties of the sequence of selenium phases: monoclinic (Se_8 rings only) ⟶ amorphous (Se_n chains plus Se_8 rings) ⟶ hexagonal (Se_n chains only) for which the absorption edge energy decreases continuously and the refractive index increases continuously.

8. During long illuminations in high vacuum photo-induced evaporation of very thin films of As_2S_3 produces a mottled structure reminiscent of phase separation as observed by TEM. The homogenization of this mottling with mild electron-beam heating indicated that the mottling can be attributed to thickness fluctuations rather than to compositional fluctuations.

9. The optical effects in As_2Se_3 and As_2S_3 can be entirely accounted for in terms of defect formation (photodarkening) and polymerization (photostructural and thermostructural changes), and no optical evidence for phase separation was obtained. Conversely, the parallel shifts of the absorption edge accompanying illumination or annealing are inconsistent with the segregation of a heavily absorbing second phase such as amorphous arsenic or with any change of light scattering which would accompany phase separation.

10. The enhanced chemical reactivity of As_2S_3 accompanying exposure to band-gap illumination, such as oxidation in a 10^{-6} torr vacuum or reaction with a thin Ag underlayer, appears to be a concomitant of the photostructural transformation, possibly involving localized electronic defects including trapped charges and broken bonds.

TABLE OF CONTENTS

1. INTRODUCTION AND SUMMARY OF MAJOR ACCOMPLISHMENTS

1.1 Introduction

As described in the Introduction to the Fourth Semi-Annual Technical report of this Research Contract, a key element in interpreting the thermal, optical and electronic properties of amorphous chalcogenide alloy films in terms of chemical bonding concepts is the determination of the role of depositional conditions, illumination and annealing in controlling the atomic structure of the deposited film. It is not adequate merely to specify the composition and the amorphous state of some particular film to fix all of its properties as a function of T, P, etc. The thermodynamic state of an amorphous solid depends on its thermal history in the sense that the lowest free energy configuration at some temperature below T_g is not usually attainable on an experimentally realizable time scale. From a chemical thermodynamic viewpoint, this means that amorphous solids are not in internal homogeneous equilibrium, and thus many structural parameters which would normally be dependent thermodynamic variables for a phase in homogeneous equilibrium become independent variables which must be specified to describe the thermodynamic state. Such structural parameters include, in principle, many familiar quantities such as atomic defects (vacancies, "dislocations", voids, bond strains, etc.) electronic defects (broken bonds, trapped charges), molecular constituency (polymer-monomer ratio, polymer chain length, bond concentrations, etc.), etc. The list of properties which may have to be specified to completely describe

the thermodynamic state of a non-equilibrium amorphous solid phase is more extensive than the experimenter's capability to quantify so many unknown variables.

Fortunately the situation is considerably relieved by the fact that, above Tg, the amorphous phase can generally maintain internal homogeneous equilibrium as external parameters are varied, so that, upon cooling from T_g to $T_1 < T_g$, the departures of the various structural parameters from their equilibrium values are primarily determined by the cooling rate and the annealing time at T_1, two easily specified factors. However, band-gap illumination at T_1 can upset this structural state in a variety of ways, mostly relating to the structural "damage" introduced into the amorphous semiconducting solid by the recombination of the photo-excited charge carriers. A simple way of analyzing this "radiation damage" is to note that the recombination event perturbs the local phonon spectrum as though the local environment were suddenly up-quenched to some higher temperature and rapidly down-quenched by thermal conduction to the adjacent material. Such local thermal spikes can have two sorts of effects:

1. If the film is already in a relatively low free energy configuration, the net effect of the thermal spike is to freeze in local order characteristic of a higher temperature. This is entirely analogous to the "fictive temperature" concept which has frequently been employed to characterize the structural state of an oxide glass in terms of its thermal history. The

fictive temperature corresponds to the temperature at which, upon cooling, the glass properties departed from their homogeneous equilibrium values, "freezing-in", in effect, the structural state at the fictive temperature. This somewhat vague concept has proven useful in characterizing the departures from internal equilibrium in oxide glasses, and will undoubtedly gain increasing significance in the chalcogenide glasses where these property differences manifest themselves as conductivity and optical transmission changes.

2. If the film is illuminated while in a relatively high free energy configuration relative to the equilibrium configuration, such as might be the case for a film deposited on a substrate held well below T_g, then the net effect of illumination and the concomitant sequence of local thermal spikes may well be to overcome the activation energy barrier which separates the initial film structure from a lower free energy configuration. In this case the net effect of illumination can be to lower the free energy and to transform the film towards the equlibrium structural state.

The present Technical Report concerns itself with such departures from homogeneous equilibrium in amorphous As_2S_3 and As_2Se_3 films. In these cases the gross structural state has been monitored by x-ray diffraction while the property changes have been monitored by optical absorption and refractive index measurements. Gross structural transformation of the slowly evaporated As_2S_3 and As_2Se_3 films have been observed, both upon

annealing near T_g and upon exposure to band-gap illumination. These gross transformations involve the polymerization of the amorphous films which are formed primarily by the condensation of As_2S_6 (or As_2Se_6) molecules. The discovery that the structure of slowly evaporated As_2S_3 films can be closely described by a hard-sphere packing of As_4S_6 globular tetrahedra provides a thorough structural characterization of these films including a highly accurate calculation of the density.

An additional topic introduced in this study involves the exposure of well annealed films of As_2S_3 and As_2Se_3 to band gap illumination, and the observation of the optical property changes which accompany such exposure. This phenomenon appears to be representative of case 1 listed above, where the effect of illumination is to raise the fictive temperature, whereas the photo-polymerization reported for the slowly evaporated As_2S_3 and As_2Se_3 films is representative of case 2, involving a free energy lowering upon exposure.

This study touches upon an interesting aspect of homogeneous equilibrium in an amorphous phase: The equilibrium among polymeric and monomeric species. For As_2S_3 and As_2Se_3, the equilibrium metastable liquid at T_g and, presumably, the ideal metastable glass below T_g are fully polymerized, and the presence of monomeric or dimeric molecular units in solid amorphous films (evaporated) is indicative of departures from this equilibrium state. However, other amorphous phases such as Se, S, and S or Se-rich glasses cross-linked by Ge or As contain a mixture of polymeric and

molecular components in the equilibrium amorphous phase. The perturbation of this equilibrium by variations of quench rate has been studied in the case of Se glasses.[5] The equilibrium between Se_8 rings and Se_n chains is apparently "frozen in" at a fixed ratio at roughly 150°C, well above T_g, and glasses annealed at all temperatures below this value have the same ring-chain ratio. Note that all of these experiments have been performed well above T_g, proving that T_g need not constitute a temperature for rapid attainment of homogeneous equilibrium in a system like Se which has strong covalent bonds along the chains and weak van der Waals bonds between the chains. For such a polymer, the T_g phenomenon involves only the excitation of the weak van der Waals bonds, so that internal equilibrium involving covalent bonds is probably established at a temperature well above T_g rather than at T_g. While these comments serve to introduce this additional aspect of internal equilibrium in solid and liquid amorphous phases, it has been the goal in our high temperature materials studies performed under the present Research Contract to avoid those alloy compositions which contain a substantial <u>equilibrium</u> concentration of monomeric constituents. This goal follows as a logical consequence of our focus upon high-temperature stability, for the role of monomer constituents is essentially that of a plasticizer, which tends to lower the thermal stability of polymeric networks in which such monomer constituents occur.

1.2 Summary of Major Accomplishments

1. Slowly evaporated amorphous films of As_2S_3 and As_2S_3 undergo structural transformations when exposed to band gap illumination (photostructural transformation) or when annealed at $\sim T_g$ (thermostructural transformation).
2. The initial structures of these evaporated amorphous solids appear to retain the molecularity which characterizes the vapor from which they are condensed.
3. In the case of slowly evaporated As_2S_3, the X-ray diffraction pattern is well characterized in terms of a dense-random packing of As_4S_6 molecular "hard-spheres", and the density calculated from this structural model agrees well with the measured density.
4. X-ray patterns of the transformed evaporated As_2S_3 and As_2Se_3 films closely resemble patterns of the sputtered films and the bulk glasses, indicating that polymerization of the molecular units occurs during the photostructural and thermostructural transformations of the evaporated films.
5. The refractive indices of the evaporated films increase irreversibly with annealing at T_g or with band-gap illumination, attaining values close to the bulk glass value for As_2S_3. No measurable change ($\Delta n < 0.01$) of refractive index accompanies illumination of the annealed films or annealing of the illuminated films.
6. The optical absorption edge energy of the evaporated films decreases irreversibly with annealing at T_g or with band-gap illumination.

A decrease of absorption edge energy accompanies exposure of the annealed films, and the edge can be reversibly restored by reannealing. This shift, termed photodarkening, is small for As_2Se_3 (~0.01 eV) and somewhat larger for As_2S_3 (~0.03 eV).

7. The irreversible optical effects accompany the irreversible structural effects, and can be qualitatively associated with polymerization, by analogy with the optical properties of the sequence of selenium phases: monoclinic (Se_8 rings only)⟶ amorphous (Se_n chains plus Se_8 rings)⟶ hexagonal (Se_n chains only) for which the absorption edge energy decreases continuously and the refractive index increases continuously.

8. During long illuminations in high vacuum photo-induced evaporation of very thin films of As_2S_3 produces a mottled structure reminiscent of phase separation as observed by TEM. The homogenization of this mottling with mild electron-beam heating indicated that the mottling can be attributed to thickness fluctuations rather than to compositional fluctuations.

9. The optical effects in As_2Se_3 and As_2S_3 can be entirely accounted for in terms of defect formation (photodarkening) and polymerization (photostructural and thermostructural changes), and no optical evidence for phase separation was obtained. Conversely, the parallel shifts of the absorption edge accompanying illumination or annealing are inconsistent with the segregation of a

heavily absorbing second phase such as amorphous arsenic or with any change of light scattering which would accompnay phase separation.

10. The enhanced chemical reactivity of As_2S_3 accompanying exposure to band-gap illumination, such as oxidation in a 10^{-6} torr vacuum or reaction with a thin Ag underlayer, appears to be a concomitant of the photostructural transformation, possibly involving localized electronic defects including trapped charges and broken bonds.

2. REFERENCES

1. J. Schottmiller, M. Tabak, G. Lucovsky and A. Ward, J. Non-Crystalline Solids 4 (1970) 80.
2. B. G. Bagley, F. J. DiSalvo and J. V. Waszczak, Solid State Comm. 11 (1972) 89.
3. S. Tsuchihashi and Y. Kawamoto, J. Non-Crystalline Solids 5 (1971) 286.
4. S. Tsuchihashi and Y. Kawamoto, J. Amer. Ceram. Soc. 54 (1971) 131.
5. A. Eisenberg and A. V. Tobalsky, J. Polymer Sci. 46 (1960) 19.

APPENDIX I

PHOTOSTRUCTURAL TRANSFORMATIONS IN AMORPHOUS As_2Se_3 AND As_2S_3 FILMS

J. P. deNeufville, S. C. Moss and S. R. Ovshinsky

Submitted to:

Journal of Non-Crystalline Solids

ABSTRACT

The influence of illumination and annealing on thin films of amorphous As_2Se_3 and As_2S_3 has been studied through their effects on the structure and optical properties. It is shown that the dominant photostructural change in evaporated films is the polymerization of the as-deposited molecular (As_4S_6 or As_4Se_6) glass through either illumination or heating. This irreversible polymerization gives rise to a large absorption edge shift to smaller energy and to an appreciable index of refraction change. In addition there is a small reversible absorption edge shift, due presumably to trapping of photo-generated electrons and holes which is larger in As_2S_3 than in As_2Se_3. This reversibility persists in both well-annealed evaporated films and in sputtered films which appear to be structurally indistinguishable both from each other and, aside from defects or voids, from the bulk glass. The reversible effect, called photo-darkening, is accompanied by a negligible refractive index change when compared with the irreversible polymerization change. The application of the present results to photochemical effects is discussed.

I. INTRODUCTION

Photochromism and image formation in glassy chalcogenide materials have recently received much attention both because of the application to the direct storage of digital information[1-3] and because of the implications for the three dimensional storage of potentially erasable phase holograms[3-9]. A variety of mechanisms have been invoked in explanation of the photo-induced optical changes some of which are: photo-flow[2] (including polymerization and depolymerization); photo-structural effects[1,3,5-8], by which is usually meant the photon enhancement of crystallization including nucleation and/or growth, or the alteration of the defect state; photo-induced chemical changes such as phase separation[3-8], oxidation[5], reaction with metals[9]; and so forth.

Among the large number of these amorphous chalcogenide alloys that have been studied, arsenic-sulfur glasses, with special emphasis on As_2S_3, and arsenic-selenium glasses, again concentrated around the As_2Se_3 composition, have been singled out as potential holographic storage media. The thermodynamic and phase relations in these alloy systems were studied by Myers and Felty[10] for the liquid and crystalline phases, including a phase diagram determination and a measurement of the glass transition temperatures, T_g, from As_5S_{95} to $As_{40}S_{60}$ (As_2S_3) and from Se to $As_{60}Se_{40}$. The As-Se phase diagram demonstrates large nonideality

along a portion of the Se liquidus which is typical of a tendency toward phase separation, and the measured T_g's show an anomalous change in slope with composition between 10% As and 30% As. There is a T_g maximum at about 43% As essentially coinciding with a well-defined melting point maximum for the crystalline compound and suggesting that at As_2Se_3 there is an ordering tendency - certainly in the crystalline solid, but also in the supercooled liquid, or glassy, phase[11].

The As-S glasses demonstrate a continuous linear increase in T_g from 5% As to a maximum at As_2S_3 while the liquidus temperature increases to a local maximum at As_2S_3, falls off to a eutectic at about 43% As and rises to a second maximum at the compound As_4S_4 (realgar). The structure of both the As_2S_3 and As_2Se_3 glasses is a subject of continuing interest. The addition of the trivalent As to either S or Se is thought to copolymerize the elements through the formation of branch points whose concentration increases with arsenic concentration to the point, at As_2S_3 or As_2Se_3, where a complete network can be formed with only As-Se or As-S bonds and no remaining elemental chain or ring segments[12].

While the crystalline phases are best described as puckered layer structures (the orpiment structure) it is not clear how best to describe the glasses. Tsuchihashi and Kawamoto[13] suggest an analogous distorted layer structure for glassy As_2S_3 based both upon a survey X-ray analysis of structures in the As-S glasses and upon optical, chemical

and thermal properties. Renninger[14] reports that no microcrystallite model yields an acceptable fit to his radial density analysis of several glasses in the range Se-AsSe although the nearest neighbor environment is identical to the crystal. He does find, however, that Monte Carlo computer fits to the structure, performed by progressively perturbing the crystal, yield both distorted layer environments, with bridging atoms to make a more 3-D network, and molecular clusters, especially for compositions near AsSe. Additional evidence for a well-preserved nearest neighbor environment comes from the NMR studies on As_2S_3[15] which give a maximum bond angle distortion of $\sim 2^{\circ}$ from the crystalline values, and from detailed analyses of the optically active modes in As_2S_3 and As_2Se_3[16].

As Brandes et al.[4] point out, the holographic effect in bulk As-S glasses arises mainly from a change in index of refraction, which Pearson and Bagley[17] attribute to crystallization of rhombic (α) sulphur crystals in As_7S_{93}. The diffraction efficiency of a stored grating falls off dramatically between 20 and 25% As, which is the same composition range in which Tsuchihashi and Kawamoto report the disappearance of the S_8 constituent in the glasses[13]. Thus the holographic response for these sulfur-rich As-S alloys seems to be associated with the presence of S_8 molecules.

The above results[4,17] represent the only data available on bulk As-S or As-Se glasses where the "film" samples were prepared by

pressing the liquid between two glass plates. The other reports on holographic storage in As_2S_3 or As_2Se_3 films are concerned mainly with optical effects in evaporated films. In As_2S_3 the most recent observations are by Keneman[6] and Ohmachi and Igo[7] while in As_2Se_3 and related glasses Igo and Toyoshima[8] have reported on the optical properties and holographic response. (Possible mechanisms for reversible photo response in both these materials had previously been discussed by Berkes et al.[5]) Ohmachi and Igo find a decrease in transmittance for evaporated As_2S_3 (photo-darkening) which disappears with decreasing As at $As_{15}S_{85}$. The diffraction efficiency of their stored grating in As_2S_3 approaches 50% whereas the Brandes et al. result was zero efficiency at this composition. Keneman also successfully stored a hologram in As_2S_3 and measured first-order diffraction efficiencies of >80%. The erasure of his stored grating was thermal and although the state to which he returned his film was not the starting one, a new grating, orthogonal to the first, could be stored and observed in transmission using an interference filter. The process was reportedly not indefinitely repeatable, due to cracking of the As_2S_3 layer.

Igo and co-workers[7,8] comment on two processes which they believe are operative in these photosensitive materials. One is primarily thermal and causes a general shift of the absorption edge to shorter wavelengths - an increase, it should be noted, in optical gap not unlike that

produced by the well-known annealing of defects in vapor-deposited thin films[18]. The other is a photo-effect and produces the increased absorption or photo-darkening usually observed. It is this process which Berkes et al.[5] identify, both in As_2Se_3 and As_2S_3, with reversible photo-decomposition which they suggest is a cycling of, say, As_2Se_3 above and below a metastable immiscibility boundary. Their evidence for this is largely in the observation of photo-enhanced oxidation of As_2S_3 with the subsequent formation of sulphur crystals.

The purpose of this paper is to delineate the photo-structural and photo-conductive processes which are associated with optical storage effects in amorphous As_2S_3 and As_2Se_3 films. An important aspect of our work is the uncovering of structural differences and optical effects associated largely with film preparation method and thermal annealing history. We have attempted to correlate optical and structural properties to obtain a consistent picture of the photoresponse which accounts for the behavior of films prepared in a variety of ways.

II. EXPERIMENTAL

A. Sample Preparation

The amorphous As-Se samples used in this study were prepared by evaporation, sputtering, or slow cooling of the liquid phase, and the amorphous As_2S_3 films were made by evaporation of the bulk glass. The evaporation sources, sputtering cathodes, and bulk glass samples were fabricated directly from high-purity oxidation-free elements melted together in evacuated silica ampoules. The bulk glass X-ray diffraction samples were annealed at approximately 200°C for 30 min ($T_g \approx 180$°C) which stress-relieved the quenched glass sufficiently to permit grinding and polishing. RF cathodes were prepared by hot pressing crushed glass powder under a dry nitrogen atmosphere at 275°C.

Sputtering was carried out in an R.D. MATHIS SP-310 module mounted on an oil pumped vacuum system. Using a 3.5" cathode, 7×10^{-3} torr argon pressure and 750 rf V we obtained sputtering rates of approximately 125 Å min^{-1}. A typical series of film thicknesses was 0.4, 1.2, 4.8 and 20μm, chosen to provide a wide range of optical absorption samples and to coincide with the thickness range obtainable by evaporation. Films of approximately 500Å thickness were sputtered onto carbon coated nickel electron microscope grids for transmission electron microscope (TEM) examination.

The evaporations were conducted in an ion-pumped oil-free system at a pressure of 5×10^{-8} torr and a deposition rate of approximately

1000 Å min^{-1} onto Croning 7059 1" x 1" glass substrates held at a distance of 20 cm from the source. We were careful to keep the source temperature as low as possible during the thermal evaporation in order to ensure a minimum of substrate irradiation or heating. Evaporated film thicknesses of 0.5 to 20 μm were used for X-ray diffraction, density, and optical transmission measurements. The 20 μm upper thickness limit for evaporated films was governed by spalling effects observed for thicker films.

The illuminations were performed in a 10^{-8} torr vacuum in order to eliminate the light-induced oxidation which has been reported for these materials[5], and which we invariably observed for thin As_2S_3 films illuminated in a poor vacuum. Transmission electron microscopic observations after UHV illumination of 500 Å thick As_2Se_3 and As_2S_3 films evaporated over carbon-coated TEM grids revealed no oxidation, although, in the case of As_2S_3, light-induced evaporation accompanied illumination. The illumination source was an Olympus tungsten filament microscope illuminator which projected a uniform 0.1 watt-cm^{-2} beam onto the substrate. We used a 0.8 μm short pass filter in the optical path which reduced substrate heating effects to an acceptable level of approximately $5^{o}C$.

The annealing treatments were performed in an opaque stainless steel enclosure using a slowly flowing atmosphere of dry nitrogen to

assure an oxygen and moisture-free environment.

B. Measurements

The sputtered and evaporated As-Se compositions were measured with an electron beam microprobe analyser in which the L_α Se and As intensities were monitored both for the thin films and for a series of bulk glass standard samples. By comparing the ratio of peak selenium counts to peak arsenic counts in the bulk standards and the film samples it was possible to determine that the As/Se atomic ratio in both evaporated and sputtered As_2Se_3 films is 0.666 ± 0.013. No analysis of the evaporated As_2S_3 films were obtained, because it is well known[19] that liquid As_2S_3 evaporates congruently without fractionation.

The X-ray intensity data were collected in the range $2\theta = 10^\circ$ to 70° with a Phillips-Norelco diffractometer using copper radiation (37 kV, 17 ma) and an A.M.R. graphite post-specimen monochromator set on the Cu K_α line. The recorder trace was fitted by a smooth curve and the data were replotted at 0.5° intervals to obtain the final curves. The reproducibility of this procedure from run to run was approximately ±2% so that the curve shape obtained was very well characterized, permitting detailed observation of the diffraction changes produced by annealing and illumination. However, variations among film sample thicknesses limited the usefulness of comparisons of absolute intensity from one set

of experiments to another.

Transmission electron microscopy (TEM) experiments were performed on stress-free carbon coated nickel grids overcoated with 500 Å of the sample film using a JEM 7 electron microscope operated at 80 kV. Optical absorption coefficients were calculated from transmission measurements obtained for As_2Se_3 with a single prism Beckman DU monochromator and a PbS photocell using synchronous detection techniques. For As_2S_3 the transmission data were obtained with a double prism Cary 11 spectrophotometer using a photomultiplier as the optical detector. The As_2Se_3 absorption data were obtained using samples ranging between 0.5 and 20 μm thickness while the As_2S_3 data were obtained with 2 - 3 μm thick samples only. The refractive index data were calculated from the exact sample thickness (2 - 3 μm, accurate to ~2%) by observing the wavelengths of the reflection maxima and minima in the transparent portion of the spectrum. The samples were exposed to band gap illumination only during the absorption edge measurements, and the absorbed exposures were of the order of 0.01 J cm^{-2}, too low to affect the most photosensitive films examined in this study.

Density measurements are listed in Table 1 for thick (~20 μm) sputtered and evaporated As_2Se_3 and As_2S_3 films and for the well annealed bulk glasses.

The film densities were calculated to ±2% accuracy by differentially weighing a film of known thickness and area. The bulk glass densities were measured to ±0.5% accuracy using the Archimedean method. We noted no change in weight or thickness accompanying exposure or illumination of the evaporated As_2Se_3 or As_2S_3 films, proving that these processes do not measurably affect the average film density or composition.

III. EXPERIMENTAL RESULTS

A. X-Ray Diffraction

1. General Comments

The X-ray diffraction effects tentatively associated with imaging in glassy material include changes in local order (such as polymerization), crystallization, phase separation into two glassy phases (followed or not by crystallization), and relaxation or densification. Crystallization may be detected in a straightforward way at a level of about 1 vol. pct. through the appearance, in the normally diffuse diffraction pattern, of sharper peaks at Bragg angles given by the interplanar spacings of the crystalline phase(s). Conventional phase separation consists of compositional fluctuations whose amplitudes and spatial extent depend upon the treatment given the initially homogeneous glass[20]. One can, for example, quench in composition fluctuations in a phase-separating glass which are then coarsened through further treatment. In the initial stages, small angle X-ray scattering provides an ideal

TABLE 1

Densities of Amorphous As_2S_3 and As_2Se_3 Samples

Sample	Density
As_2S_3	
Bulk	3.195 ± 0.15
Evaporated	3.27 ± 0.06
Sputtered	3.23 ± 0.06
As_2Se_3	
Bulk	4.58 ± 0.02
Evaporated	4.31 ± 0.08
Sputtered	4.29 ± 0.08

probe of the Fourier spectrum of electron density fluctuations that accompany the composition excursions, and transmission electron microscopy of thin samples can reveal the morphology of the separation directly. Neither of these methods will be particularly sensitive to composition fluctuations in the As-Se system because of the similarity in electron density of As (Z = 33) and Se (Z = 34), but the methods are useful for As_2S_3. At a later stage in its development, phase separation may change in character from the composition modulation of a single glassy structure to the development of two distinct structures with a diffraction pattern given by the superposition of the separate patterns.

Densification of a vapor-deposited sample can be detected through a decrease in scattering from free volume, voids, bubbles, etc., and is usually observed at angles well below the first diffuse peak in the X-ray interference function[21]. This is not so much an intrinsic structural change as a removal of zero-density scattering regions, but it may lead to a change in optical density through the sharpening ot the absorption edge and the removal of defect states within the energy gap of the amorphous semiconductor[18].

2. Results

Our initial X-ray experiments were concerned with the possible alteration in the structure of amorphous As_2Se_3 upon illumination. As

noted above, As_2Se_3 would be a particularly poor candidate for an X-ray study of phase separation. X-ray detectable photo-structural effects in As_2Se_3 would thus be mainly confined to a relaxation or alteration of intrinsic local glass structure, to an incipient crystallization or to densification. Fig. 1 presents what is perhaps the major result of our structural study in which the influence of illumination by a white source (tungsten lamp) on vapor-deposited As_2Se_3 is compared with a thermal treatment of the same material. Fig. 1(a) shows the X-ray diffraction pattern from a film of about 2 μm thickness, deposited over a Corning 7059 plate, in the as-deposited state and after a 17 hour illumination at room temperature. Associated with this treatment is an appreciable photo-darkening as will be described in greater detail in the discussion of the optical property measurements. While a small portion of this optical densification can be bleached by heat treatment at $T_g = 180^oC$ for one hour, the X-ray trace following this heat treatment, as also shown in fig. 1 (a), shows no reversal to the as-deposited structure.

Because the films in fig. 1 are ~ 2.0 μm thick the angular dependence of the intensity is not that of a thick film. At lower glancing angles ($2\theta < 30^o$) the condition of near infinite thickness is increasingly approximated, but at larger angles, the X-ray beam samples less of the As_2Se_3 and more of the 7059 plate. The result is a more rapid fall-off in the As_2Se_3 pattern and, among other things, the appearance of a weak bump at $2\theta \cong 41^o$ which is the second strong diffuse peak from

the 7059 substrate. The first peak from the 7059 substrate ($2\theta \cong 25^{\circ}$) is not so observable because of the greater effective thickness of As_2Se_3. We will, however, present data showing that the thin film results were not modified in any important way by going to thicker films.

The principal effect in fig. 1(a) is the change in the entire scattering pattern upon illumination. The first sharp diffuse peak is reduced by a factor of 2 in intensity, is rendered almost twice as broad, and is shifted to higher angle; the minimum at $2\theta \cong 20^{\circ}$ is lifted; the second diffuse peak changes its shape and is shifted to higher angle; the third diffuse peak is shifted slightly, and so forth. What we are observing in fig. 1(a) is a structural alteration that cannot be attributed simply to phase separation and is not due to crystallization. The change proceeds progressively with illumination from the as-evaporated film pattern to the final pattern, with the first sharp diffuse peak gradually approaching the profile in the exposed pattern of 1 (a). Once the exposed level is achieved, heating does not return the film to the virgin state.

Fig. 1(b) demonstrates the reverse cycle - namely the heating or annealing of a virgin film at its glass transition temperature ($T_g = 180^{\circ}C$) followed by illumination at room temperature. The result is clearly that both heating and illumination produce the same structural change in an as-deposited evaporated film of As_2Se_3, and that this structural effect, which carries with it an attendant optical density change, is not reversible. For the films in fig. 1(b) the optical density increase on

annealing was comparable to the darkening of fig. 1(a).

Fig. 2 shows an identical effect on annealing for an evaporated 22 μm As_2S_3 film in which the progressive decrease, broadening and shifting of the first diffuse peak is apparent. (As_2S_3 is more transparent to X-rays and the 7059 substrate peak at $2\theta = 41^{o}$ is still observable, even at a film thickness of 22 μm.) Again there is no evidence for phase separation; rather we note a dramatic relaxation or change in the entire structure comparable to that of fig. 1(b). Essentially, the same effect is obtained with illumination as in fig. 1(a), but self-absorption of the illumination by the 22 μm As_2S_3 film results in a gradient of the degree of structural transformation versus thickness for 17 hours illumination. The results in figs. 1 and 2 seemed striking enough to us to suggest additional experiments by which the structural changes could be delineated. Since it is difficult to obtain direct structural information from the intensity function, we would hope in the future to perform selected radial density analyses either on the two structural states represented in figs. 1 and 2 or on the difference function given by their subtraction. However, because the intensity profile of the first diffuse peak decreases, broadens and shifts, we can conclude that substantially more than nearest correlations are involved in the change. It is not, in other words, merely a variation in nearest neighbor identity or coordination but rather a much more dramatic or systematic alteration of the longer range structure, which we will presently discuss.

Noting that the effects of annealing and illumination were nearly identical and essentially non-reversible, we collected the thick (22μ) film As_2Se_3 data in fig. 3. The 7059 substrate bump at $2\theta = 41^\circ$ has disappeared and the data are better determined at higher angles, but the major results of fig. 1 remain unchanged. The distinction between sputtering and evaporation was then explored because initial observations on sputtered films of As_2Se_3 showed only a very weak photo response. By this we mean that the diffraction efficiency of a stored plane grating in sputtered As_2Se_3 was more than 2 orders of magnitude less than the efficiency with an evaporated film[22]. Fig. 4 presents the X-ray scattering from a sputtered 10.9μ film of As_2Se_3 over 7059 both before and after a one hour anneal at 180°C. There is essentially no difference in structure in this case and very little evidence in the X-ray scattering below $2\theta = 12^\circ$ for any densification accompanying the annealing, the latter result being similar to evaporated film data. The diffraction patterns in fig. 4 are very similar to the diffraction patterns of annealed evaporated As_2Se_3 in fig. 3. A similar result was obtained for sputtered As_2S_3. This similarity in structure between sputtered films and annealed (or fully illuminated) evaporated films presumably is why the sputtered films show such a weak photo response and demonstrate no structural change.

Finally, we explore in a qualitative way both the structure of bulk As_2Se_3 glass and the influence of compositional variations on the X-ray scattering from As-Se glasses in the vicinity of As_2Se_3.

Fig. 5 shows the diffraction patterns from polished bulk samples of the compositions $As_{35}Se_{65}$, $As_{40}Se_{60}$ (As_2Se_3) and $As_{45}Se_{55}$. The bulk As_2Se_3 sample shows a pattern essentially identical to the annealed or illuminated evaporated films (figs. 1 and 3) and the sputtered films of fig. 5. In all four of these diffraction patterns the relative heights of the diffuse maxima and minima are the same and they occur at the same respective values of 2θ. The change with composition demonstrates variations that remind us of aspects of the as-evaporated film, especially at $As_{45}Se_{55}$, where the first peak is shifted to lower angle and the minimum at $2\theta = 20^{\circ}$ is deeper. The rest of the pattern in $As_{45}Se_{55}$ is similar to the diffraction results on the other samples and unlike the evaporated films. Our microprobe analysis on the latter films makes it clear, in any case, that we do not have composition changes accompanying the evaporation of As_2Se_3.

B. Electron Microscopy (TEM)

TEM was performed on 500Å films of As_2S_3 evaporated onto carbon coated grids and examined both before and after in situ illumination in the 10^{-8} torr vacuum in which they were deposited. Figs. 6 and 7 show the results. Fig. 6(a) is the TEM image of a film evaporated but unexposed, i.e., it is the shadowed half of the grid whose illuminated portion is shown in fig. 6(b). Fig. 6(b) bears a remarkable resemblance to a phase separation morphology in that the pattern of electron dense and electron transparent regions seems fully interconnected[20]. The

scale of mottling in 6(b) is on the order of 1200 - 1500Å. Were it to consist of As-rich and S-rich regions, it would thereby appear in the corresponding X-ray diffraction pattern as the superposition of two glassy patterns which would merge during a homogenization anneal to a single glassy phase.

Fig. 6(c) is a TEM photo taken after a gentle warming of the film under electron-beam illumination in the microscope. It was our hope to anneal out the mottled structure of 6(b) but in the process of so doing small bubbles invariably formed in the dark, or electron dense, regions. These bubbles appear to involve the selected volatilization of a molecular species (they are morphologically quite similar to argon bubbling near T_g in sputtered films) which is either the As_2S_3 itself or a minor constituent present in very small amounts. The latter is inferred from the fact that the thicker films do not change composition, as determined by weighing, after either the illumination or thermal treatments in figs. 1-3.

Two alternative mechanisms which might account for the electron beam induced homogenization of the mottled structure seen in fig. 6(b) involve smoothing of film thickness fluctuations or smoothing of lateral compositional fluctuations. We feel that the bubble formation which accompanies the early stages of this homogenization is indicative of a relatively low film fluidity which would be sufficient to permit some viscous flow on a scale of 1000Å but insufficient to permit diffusional

transfer of material on the same scale. The formation of the bubbles in the electron dense regions of the film is also consistent with these regions having a greater thickness than the adjacent less electron dense regions. Bubble nucleation can occur when a minimum internal pressure of the volatilizing species is exceeded. Evaporation from the free surface of the film acts to deplete this pressure, and the depletion is more effective for the thinner portions of the film.

Fig. 7 shows the electron diffraction pattern of the exposed film, which contains only amorphous bands and no sharp crystalline rings. We could not visually distinguish any changes in electron diffraction after illumination. If the electron beam did not transform the unilluminated area during our TEM observations, then quantative densitomitry might reveal differences in electron diffraction analogous to our x-ray results. There is certainly no evidence of crystallization (rhombic sulphur) or oxidation (As_2O_3) accompanying illumination in high vacuum.

Proceeding very carefully with the electron beam heating we can, as noted above, return the film to a condition similar to, though not identical with, that shown in fig. 6(a). Additional heating produces a further mottling on a scale coarser than in fig. 6(b) but otherwise similar. Continued heating volatilizes the entire film. Alternatively we can evaporate the film through continued <u>in situ</u> illumination. In fact our early attempts to record photo effects in the thin films resulted in a complete photo-evaporation of the films.

We therefore believe that the mottling observed in fig. 6(b) is the direct result of a photo-induced evaporation of the As_2S_3 film.

The texture is a natural and familiar consequence of the uneveness in surface topology that accompanies evaporation. It is not to be confused with phase separation, for which there is, not surprisingly, very little evidence in these materials. (Were phase separation to occur, the sulphur-rich phase would certainly be the more likely to volatilize and thus to give rise to the bubbling of fig. 6(c). In fact, however, the bubbles appear in the electron dense regions which would correspond to the arsenic-rich, rather than sulphur-rich, phase.)

C. Optical Properties

The absorption edge and the near infra-red refractive index of evaporated As_2Se_3 and As_2S_3 samples were measured before and after illuminating and annealing experiments identical to those described in the X-ray experimental section. Inasmuch as the optical properties are demonstrably affected by X-ray exposure, separate samples were used for the optical measurements. In addition, the effect of thermal annealing on the optical absorption edge of sputtered As_2Se_3 was measured to compare with the X-ray annealing experiment performed on this material.

The results of these annealing and illumination experiments are shown in fig. 8 and Table 2 for evaporated As_2S_3 and As_2Se_3. The refractive index of As_2S_3, measured at a photon energy of 1.5 eV, increased by $\Delta n \approx 0.1$ upon annealing or exposure, and the As_2Se_3 refractive index, measured at a photon energy of 1.0 eV, increased by $\Delta n \approx 0.06$ under the same conditions. While n increased slightly more after illumination

TABLE 2

Index of Refraction of Amorphous As_2S_3 and As_2Se_3

Sample	Refractive Index n	Δn
As_2S_3		
as evaporated	2.42 ± 0.05	
after exposure	2.53 ± 0.05	+0.107 ± 0.01
after annealing	2.51 ± 0.05	+0.092 ± 0.01
bulk	2.528	
As_2Se_3		
as evaporated	2.77 ± 0.05	
after exposure	2.83 ± 0.05	+0.062 ± 0.01
after annealing	2.83 ± 0.05	+0.058 ± 0.01

than after annealing for both alloys, differences are small compared to the experimental uncertainty. For As_2S_3 the refractive indices after annealing and illumination are comparable to the bulk glass value. The optical absorption edge shifts laterally to lower energies upon annealing and shifts further in the same direction upon illumination. For each evaporated material, the three absorption edges are closely parallel, showing that a band edge shift accounts entirely for the observed photodarkening and thermal darkening phenomena, and no additional scattering or absorbing second phase is indicated.

Comparing fig. 8(a) and 8(b), we note that the absorption edge of annealed As_2S_3 lies roughly midway between the initial absorption edge and the exposed absorption edge, while in As_2Se_3 the effects of annealing and exposure produce quite similar absorption edge shifts. Thus for evaporated As_2S_3, the exposed and annealed films which differ significantly in absorption have the same refractive index at 1.5 eV, while for evaporated As_2Se_3 the exposed and annealed films have comparable absorption edges and refractive indices measured at 1.0 eV.

In fig. 8(c) the direction of the small shift in optical absorption of sputtered As_2Se_3 accompanying annealing is opposite to the shift for the evaporated films. The former is the typical direction of absorption edge shifts for sputtered chalcogenide alloy films deposited well below T_g [11] and is consistent with the absence of any large structural changes accompanying the annealing of this material as shown by the diffraction

patterns in fig. 4. In this context it is important to observe that the absorption edge of annealed sputtered As_2Se_3 shown in fig. 8(c) coincides essentially with the absorption edge of annealed evaporated As_2Se_3, which is replotted in fig. 8(c) for comparison. Not only are the X-ray diffraction patterns after annealing comparable (see figs. 3 and 4), but the optical absorption edges are as well.

In order to ascertain the temperature dependence of the thermally induced optical changes in As_2Se_3 we performed thermal cycles from 25°C to successively higher annealing temperatures using weak 6328 Å He-Ne laser illumination to monitor the structural transformation via its optical manifestation. These results are shown in fig. 9. Of course the dominant effect in this experiment is the temperature dependence of the optical transmission, and the irreversible optical densification (called thermal darkening) is superimposed on this effect. Note that reversible temperature-transmission cycles are obtained from 25°C to 105°C (points A-E), but that cycles to 145°C (points E-H), 155°C (points (H-K), and 175°C (points K-N) produced largely irreversible optical densification as monitored at 25°C.

The thermal darkenining appears to saturate at roughly 175°C, although time dependent transmission changes at 25°C tended to obscure the precise identification of the saturation temperature. For example, a small recovery or bleaching at 25°C was observed after the 18 hour interval which separated points N and O in fig. 9. This effect was commonly observed after both photo and thermal experiments and constitutes a spontaneous relaxation of a small portion of the optical densification

during 25°C annealing cycles. This phenomenon introduces a small experimental uncertainty in optical absorption edge measurements which depends on the time interval between annealing or exposure and the optical measurement.

In order to follow simultaneously the concomitant photostructural and photodarkening effects in evaporated As_2Se_3 films, we performed an illumination at 25°C with an incandescent exposure of 0.5 watts cm^{-2} while monitoring the 6328Å transmission with a weak He-Ne laser beam. At several intervals during the experiment we interrupted the exposure to perform an X-ray determination of the state of structural evolution, using the ratio of the intensity of the first diffuse diffraction peak I_1 ($2\theta_1 \cong 16^\circ$) to the intensity of the first diffraction minimum I_2 ($2\theta_2 \cong 22^\circ$) as a measure of the structural state.

These results are plotted in fig. 10, and show that the photostructural and photodarkening effects occur simultaneously. Furthermore, they indicate that the X-ray diffraction experiments performed at points A, C, F and H resulted in photodarkening to points B, D, G and I respectively. The bleaching from point E to point F occurred during an overnight interruption in the exposure and is comparable to the spontaneous bleaching observed in fig. 9 between points N and O.

The initial two minutes of exposure resulted in some optical densification without any detectable structural change. However, further exposure produces simultaneous optical densification and photostructural

response, and the exposure which produces the majority of the structural change coincides in time with the exposure which produces the majority of the optical densification.

Reversibility of the photodarkening of evaporated amorphous As_2S_3 and As_2Se_3 was attempted by the standard anneal for one hour at 180°C. Careful measurements of the absorption edge so obtained gave good agreement in both cases with the absorption edge measured for unexposed films after comparable annealing. Furthermore, re-exposure of the annealed films gave optical absorption edges which were in good agreement with the absorption edges measured for unannealed films after comparable exposure. Thus the absorption edges shown for annealed and exposed As_2S_3 and As_2Se_3 films in fig. 8 can be cycled reversibly by repeated exposure and annealing treatments. For As_2S_3 this reversible optical absorption shift is relatively large (ca. 0.03 eV) while for As_2Se_3 it is relatively small (ca. 0.01 eV). Furthermore, the refractive index changes accompanying these reversible cycles are quite small, ($\Delta n \approx 0.01$), or close to our minimum detectable level.

We also considered whether the early stages of photodarkening of evaporated As_2Se_3 might be reversible, inasmuch as the initial darkening stages in fig. 10 were not accompanied by any detectable change in the X-ray diffraction pattern. To resolve this question, we took an evaporated film of amorphous As_2Se_3 and exposed it to a level of 6328Å He-Ne laser

illumination which slowly produced photodarkening. After a small portion of the photodarkening response had occurred we interrupted the exposure with a ~5 min thermal cycle to 105°C, a temperature which produces no detectable thermal darkening of the unexposed film, as indicated in fig. 9.

The results of this and several subsequent exposure and annealing cycles are plotted in fig. 11. Apparently the initial effects of exposure and annealing are cumulative and no thermal bleaching is observed at first. After several exposure-annealing cycles the annealing begins to contribute a bleaching effect, and a fair degree of reversibility is obtained. However, the gradual effect of the cumulative exposure and annealing throughout the time scale of this experiment was to increase the optical density at a diminishing rate, and the experiment was not pursued to the anticipated limit of a small but completely reversible optical densification and thermal bleaching cycle.

IV. DISCUSSION

A. Structural Considerations

As noted earlier, the principal structural effect is the dramatic change in the X-ray diffraction patterns in figs. 1 - 3 as the freshly evaporated films are annealed or illuminated. It is clear from these results that annealing and illumination produce essentially the same structural alteration, although there is a small additional consequence of illumination of a fully annealed sample (i.e. darkening) which is reversible on further annealing. We thus want to separate our discussion of these optical effects into those associated with the gross structural change and those which are truly reversible. The difficulty in doing this is that the structural and non-structural aspects are coupled as in fig. 9-11. In the freshly deposited films there may be an appreciable optical effect, intrinsic to these films, that is not due to the structural change. But attempts to reverse the initial stages of that effect, i.e., to bleach the film, produce a structural alteration, and attendant darkening, that renders the non-structural photo-response weaker. Designing the proper photo response into a film then becomes a question of stabilizing the sensitive structure against alteration during the thermal reversal or bleaching without sacrifice of the photo response itself.

The dominant photo-sensitive structure is clearly that of the deposited evaporated films in figs. 1 - 3, and our problem reduces to the

elucidation of this structure and its relation to the well-annealed bulk glass structure. While the entire diffraction pattern changes on illumination or annealing the most remarkable change is in the vicinity of the first diffuse peak, at about $2\theta = 16^{o}$ for both As_2Se_3 and As_2S_3. In the virgin evaporated films this peak is quite sharp. If we were arbitrarily to associate a particle size, for example, with the breadth of the first As_2S_3 peak via the Scherrer formula: $L = 0.9\lambda/B(2\theta) \cos\theta$ (where L is the average particle size in Å, λ is the X-ray wavelength (1.54Å), θ is the angle at which the peak occurs ($\theta \approx 8^{o}$) and $B(2\theta)$ is the full width in radians at half maximum above background) we would have $L \cong 40$Å. It is of course improper to assign a crystallite size to a glass and we do not ascribe more meaning to this assignment other than to note that very long range correlations are implied by the sharpness of the coherent scattering peak at that value of 2θ. In fact it is to our knowledge as sharp a diffuse peak as has ever been reported for a glass. If the glass were really composed of crystallites of that size there would be very much sharper and more detailed structure in the scattering at larger angles.

The other noteworthy aspect of the first diffuse peak is its position. The position $\theta \cong 8^{o}$ corresponds to $r = (2 \sin\theta/\lambda)^{-1} \cong$ 5.5 Å which is substantially larger than any nearest or next-nearest neighbor spacing in the glass. We are thus faced with a very sharp diffuse peak at a low angle (large r) which washes out on annealing or illumination.

For our analysis of this change it is in many ways much better to work in k-space ($k = 4\pi \sin\theta/\lambda$) than in real space. The transformation between the two is performed in the usual way by normalizing the intensity data, $I(2\theta)$, at large k to the independent scattering curve in order to put I(k) in absolute units. For binary, or more complex glasses, the analysis is more involved[23] but is simply illustrated by the Fourier transform of the appropriately weighted scattering function:

$$F(k) = k\left[\frac{I(k)}{\langle f^2\rangle} - 1\right]$$

$$= \int_0^\infty 4\pi r\,[\rho(r) - \rho_o]\sin kr\,dr \qquad (1)$$

$$G(r) = 4\pi r\,[\rho(r) - \rho_o] = \frac{2}{\pi}\int_0^\infty F(k)\sin rk\,dk.$$

$\langle f^2 \rangle$ is the properly weighted average of the square of the scattering factors, $\rho(r)$ is the radial atomic density (atoms/vol.) and ρ_o is the average atomic density. The familiar radial density function (RDF) is given by $4\pi r^2 \rho(r)$ while the pair distribution function W(r) is the ratio $\rho(r)/\rho_o$. In the process of reducing the data to get $\rho(r)$, the higher angle, large k, scattering is weighted much more than the low k data with the result that in the above transform the first diffuse peak makes an almost negligible contribution and could be ignored as far as the first few oscillations in $\rho(r)$ are concerned. This is another way of saying that the sharpness of the first peak in I(k) in these glasses is associated with longer range correlations and not with near neighbors.

We believe that the clue both to the structure of the evaporated glasses and to the ensuing relaxation on annealing or illumination lies in the molecular nature of the vapor phases of As_2S_3 and As_2Se_3. To quote Wells[24] on As_2S_3: "Crystalline orpiment has a layer structure of essentially the same kind as the monoclinic form of As_2O_3, but vaporizes to As_4S_6 molecules with the same configuration as As_4O_6. In the As_4S_6 molecule As-S = 2.25 ± .02Å, As-S-As = 100° ± 2°, and S-As-S = 114° ± 2°. In crystalline orpiment the mean As-S bond length is 2.24Å and the mean bond angles for both S and As are 99°." The As_4S_6 molecule, which is shown in Fig. 12, we associate by straightforward analogy with As_4Se_6 as well.

Upon evaporation, As_4S_6 (or As_4Se_6) molecules are deposited on the substrate to form a molecular glass. (Other molecular species, especially in the evaporation of As_2Se_3[25], are present in significant concentrations as well, but will be ignored to simplify the following discussion.) This glass can be viewed as the dense random packing of As_4S_6 molecules which only occasionally cross link. There is a simple relationship between such a hard sphere molecular glass and the dense random packing of hard spheres which has recently been invoked in the discussion of the structure of metallic glasses such as Ni-P and Pd-Si[26]. From Fig. 12 we can see that the As_4S_6 molecule has T_d point symmetry being essentially an As tetraheron with the attached S atoms making it more spherical. In interpreting the present result of a very

sharp diffuse peak at $2\theta \approx 16^{o}$ we shall thus refer to analogous results on the metallic glasses prepared by splat cooling[27] or electrodeposition[28] for which the Bernal hard sphere model has been shown[26] to be the appropriate structure. These glasses are characterized typically by an oscillatory intensity function, I(k), in which the first peak is very intense and rather sharp, though not so sharp as in As_2S_3. As Cargill[28] points out, crystallite models fail in this case because any attempt to reproduce the sharpness of the first peak puts too much structure in I(k) at larger k. The Fourier transform of the intensity, as in Eq. (1), gives a W(r) which for nearly all the metallic glasses has a sharp first peak at the position of the hard sphere diameter 2σ, where σ is the radius of the metal atom, and a split second peak with almost-periodic repeating oscillations after that. The period of these oscillations at higher r approximates the hard sphere diameter.

The determination by Finney[29] of the RDF of a hard sphere model reproduces all of these features, including the important splitting of the second neighbor peak. While there is a slight ambiguity associated with the assignment of a hard sphere diameter based either on the nearest neighbor distance or the fit of Finney's calculation to larger r in W(r), it is generally agreed that the overall fit is remarkably good. We would like,therefore, to associate features of the intensity function I(k), or F(k), with W(r) in an effort to understand how the dense random packing of hard spheres gives rise to certain unique features in I(k) such as a

sharp diffuse peak at, say, k_1. In the first place, the most prominent distance in the structure is 2σ, the hard sphere diameter, and the W(r) function can almost be represented, if one ignores the splitting of the second peak, by a single oscillatory function somewhat like $\sin rk_1/rk_1$ which has maxima other than at r = o at $k_1 r \cong (4n+1)\frac{\pi}{2}$ n = 1, 2, .

For the first maximum in r at 2σ we have:

$$k_1 (2\sigma) \cong 5\pi/2 \tag{2}$$

or

$$\left.\frac{4\pi \sin\theta}{\lambda}\right)_1 \cong \frac{5\pi}{2(2\sigma)} \tag{2a}$$

and

$$\left.\frac{2 \sin\theta}{\lambda}\right)_1 = \frac{1.23}{(2\sigma)} \tag{2b}$$

rather than $1/2\sigma$ as might initially have been thought.

The above relation is certainly not an exact one because there is more detail in W(r) for the dense random packing model and there are thus further oscillations in I(k) and not just a sharp peak at k_1. But the observation of multiples of 2σ in W(r) does lead directly to a peak in I(k) whose sharpness is due simply to the adding in of higher harmonics in (2σ). We can construct the same function in k space, where it is more appropriate, to demonstrate this. Again:

$$\frac{F(k)}{k} \cong \sum_n \frac{\sin 2n\sigma k}{2n\sigma k} \tag{3}$$

Considering just the contribution from n = 1, we have

$$\frac{F(k)}{k} = \frac{\sin 2\sigma k}{2\sigma k} \qquad n = 1 \qquad (3a)$$

which has its first peak, at $k = k_1$, for $k_1 (2\sigma) \cong 5/2 (\pi)$. This peak is broad, but adding in the appropriate harmonics (n = 2,3,...) sharpens it. Sinha and Duwez[30] noted this constancy of the product $k_1 (2\sigma)$ which they found by observation on many glasses to be about 8.0 ($\frac{5\pi}{2} = 7.85$), and used their empirical rule to evaluate the nearest neighbor distances for glasses whose transform they did not take, and Giessen and Wagner[23] discuss the general application of the above Ehrenfest relation, in Eq. (2), to metallic glasses. Applying this simple analysis to the Ni-P glasses of Cargill[28], we note that the first sharp peak in I(k) occurs at $k_1 = 3.08$. If $k_1 (2\sigma) = 2.46\pi$, $2\sigma = 2.51$ Å which is the hard sphere diameter obtained by fitting W(r) to Finney's calculated W(r).

Because the metallic glasses are densely packed they resemble, in some ways, cubic close packed metals with a nearest neighbor coordination of about 12 for both. It has therefore in the past been tempting to try to associate features of their diffraction patterns with the scattering from f.c.c. crystallites. The first peak in I(k) then becomes the

(111) peak of the tiny f.c.c. crystallite. The relationship of the spacing d_{111} to 2σ as in Eq. (2) shows how this confusion can arise[23].

In applying these arguments to As_4S_6 or As_4Se_6 we use only the fact that they are deposited as molecules with a well-defined diameter. All of the low r information on interatomic correlations that is revealed in the RDF by the transform of F(k), such as distances and coordinations, is ignored. The only feature of I(k) that concerns us is the sharp first peak. We shall use the As_2S_3 glass because its peak is sharper than the corresponding one in As_2Se_3 suggesting that on deposition there is partial polymerization of the molecular constituents[25] of the gaseous selenide. The peak in As_2S_3 comes at $2\theta = 16.1^{\circ}$ corresponding to a value of $2 \sin\theta/\lambda = .182 = 1.23/2\sigma$ using the relationship between k_1 and 2σ which applies to the Ni-P glasses[28]. 2σ thereby is equal to 6.77 Å and $\sigma = 3.39$ Å. Taking this value for the hard sphere radius, we can calculate the hard sphere volume as 162.5×10^{-24} cm^3/molecule. Finney[29] measured the volume fraction of free space in his hard sphere model to be 0.36, giving a packing density of 0.64. Dividing the As_4S_6 hard-sphere molecular volume by the packing density gives 253.9×10^{-24} cm^3/molecule as the volume per As_4S_6 molecule in the assumed hard sphere glass. The weight per As_4S_6 molecule is 81.69×10^{-23} gm, and the calculated density is thus 3.21 gm/cc. We would estimate this prediction to be good to within perhaps 5 - 10% because of uncertainties

in measuring the density to compare with it. Given all of that, it is remarkably close to the measured value for the evaporated films of As_2S_3 of 3.27 gms/cc., especially since the density varies as $(2\sigma)^3$.

Our interpretation of the principal structural effects becomes quite simple. The freshly deposited evaporated film is a molecular glass with, for As_4S_6, a hard sphere diameter of about 6.77 Å. Noting that the metallic glasses have oscillations in W(r) out at least to $6(2\sigma)$, we would estimate a molecular correlation range here of about 6(6.77) or approximately 40 Å in good agreement with the rough calculation based on the Scherrer formula. The larger the molecule in a hard sphere glass, the sharper the first peak will be. As relaxation takes place the molecules begin to cross link to form the network structure of the bulk glass: i.e., the monomer polymerizes. This happens either upon illumination or upon annealing and destroys the long-range oscillatory hard-sphere-glass W(r), which in turn leaves fewer harmonics contributing at k_1, and thus a washed-out or broadened first diffuse peak. Its position and breadth gradually merge into the first peak of the bulk glass structure and it would still be interesting to provide an interpretation of such a well-defined low k feature for the polymerized glass.

We must also consider as part of the structural discussion the proposed mechanism of Berkes et al.[5] for the photo-response of these materials. Their interpretation of the semi-reversible photodarkening was in terms of a photo-dissociation of the As_2Se_3 or As_2S_3 structure into Se-rich (or pure S) regions and As-rich regions. The amorphous sulphur so produced would, on prolonged illumination, convert to rhombic sulphur while the arsenic oxidized to As_2O_3 in the presence of O_2 or H_2O. We have consistently observed as well that thin films (~500 Å) of As_2S_3 when illuminated in poor vacuum showed in the TEM, As_2O_3 crystals in a fine dispersion on the surface. Apparently there is a strong photo-catalyzed arsenic oxidation, depleting the glass of arsenic, and leaving behind S_8 rings which crystallize. The question arises as to whether such oxidation is preceded by fine scale phase separation (i.e., glass-in-glass immiscibility).

The X-ray results presented in figs. 1 - 3 were addressed to this question. The As_2Se_3 pattern would, of course, not be sensitive to phase separation <u>per se</u> but would certainly demonstrate structural changes if the phase separating species had different structures on a local scale as in Fig. 5. As_2S_3 would show both the traditional increase in low angle scattering and the larger angle structural changes that might be inferred from the results on $As_{2-x}Se_{3+x}$ in Fig. 5. Furthermore, these changes would be reversible through thermal treatment above the proposed miscibility line. The TEM results on As_2S_3

illuminated in vacuo after deposition would also be instructive.

From figs. 1 - 5 we arrived at the inevitable conclusion that phase separation is not a factor in these glasses. The as-deposited glasses start out as the dense packing of As_4S_6 (or As_4Se_6) molecules and anneal to the bulk, or sputtered, structures. Further illumination or annealing in any sequence produces no further structural alteration, aside from the familiar defect creation and annealing. The TEM study of As_2S_3 might initially be interpreted as phase-separation into two glassy phases. The scale, however, would have to be ~1000Å and would have to be reversible under thermal treatment. None of this is compatible with figs. 1 - 6. Instead, as we noted earlier, the mottling in the TEM is associated with thickness fluctuations caused by photo-evaporation, and the electron-beam induced "homogenization" is associated with the smoothing of these thickness fluctuations.

B. Optical Effects

We begin the analysis of the optical changes accompanying the photostructural and thermostructural transformation of evaporated As_2S_3 and As_2Se_3 by noting that all the absorption changes involve only lateral shifts of the absorption edge, with no evidence for increased scattering or other optical effects which would affect the slope of the absorption edge. This result is confirmed by careful examination of the optical transmission curves themselves, which indicate no detectable scattering or absorption losses at long wavelengths either in the virgin films or after annealing or exposure. These observations are consistent with the experimental results of Keneman[6] for evaporated As_2S_3 and of Berkes et al.[5] for evaporated As_2Se_3, although the latter authors interpret their photodarkening results in terms of the precipitation of heavily absorbing As clusters.

The refractive index data presented in Table 2 show that n(1.5 eV) for evaporated As_2Se_3 and n (1 eV) for evaporated As_2S_3 change considerably after annealing or illumination, indicating that the $\epsilon_2(E)$ spectrum in the vicinity of the lowest interband transition energy (~4.7 eV for As_2S_3, and ~3.8 eV for As_2Se_3, both corresponding to lone pair to conduction band excitations[31]) is significantly perturbed by the structural transformations (polymerization) which accompanies these treatments. By contrast, the refractive index is essentially unchanged (within the experimental uncertainty of $\Delta n = 0.01$) after illumination of the annealed films, even

though the absorption edge is shifted. These latter reversible photodarkening and thermal bleaching phenomena, which are most dramatic for As_2S_3 involving a reversible absorption edge shift of 0.03 eV, are therefore accompanied neither by structural changes, as monitored by X-ray diffraction, nor by significant changes in the $\epsilon_2(E)$ spectrum, as monitored by $\epsilon_1 = n^2$ in the transparent portion of the optical spectrum.

The refractive index of bulk As_2S_3 glass has been analyzed in terms of the Wemple and DiDomenico[32] (W-D) formalism by Wemple[33] and by Galkiewicz and Tauc[34]. This formalism gives the dispersion relationship for $\epsilon_1(\omega)$ between the absorption edge and the lattice vibration band in terms of two parameters, E_D and E_o, which characterize the strength and resonance frequency of a one-oscillator fit to the lowest interband transition in $\epsilon_2(\omega)$:

$$\epsilon_1(E) = n(E)^2 = 1 + E_D E_o/(E_o^2 - E^2). \qquad (4)$$

Galkiewicz and Tauc obtained agreement between this equation and the n(E) data of Rodney et al.[34] for amorphous As_2S_3 in the energy range 0.4 - 2 eV using the parameters $E_o = 4.7$ eV and $E_D = 22.8$ eV. This value of E_o is in close agreement to the energy of the first peak in $\epsilon_2(\omega)$ of 4.8 eV obtained by Drews et al.[31] for this material, and gives an indication that the first peak in $\epsilon_2(\omega)$, which corresponds to the non-bonding (lone-pair) to anti-bonding interband transition, can be associated with the single oscillator frequency in this material.

Since we measured n at fixed photon energy, rather than as a function of photon energy, we are unable to assess the relative importance of changes

of the interband oscillator strength and changes of the oscillator energy in accounting for the observed changes in refractive index. However, our preliminary analysis of n(E) indicates that a decrease in E_o by ~0.2 - 0.3 eV rather than an increase in E_D is the dominant effect for both As_2Se_3 and As_2S_3. We note by analogy that the first peak in ϵ_2 for molecular monoclinic selenium crystals occurs at 4.25 eV[36] while the same peak for the linear polymeric hexagonal selenium crystals occurs at 3.4 - 3.9 eV, depending on orientation[37]. Glassy Se which contains both rings and chains[38] has its first peak in ϵ_2 at ~4.1 eV[37], midway between the hexagonal and monoclinic crystalline values. Since all three Se phases have essentially the same nearest neighbor separation[39,40], these shifts of ϵ_2 accompanying polymerization appear to derive from changes in hybridization of the lone-pair electron band accompanying structural change, rather than from changes within the bonding or antibonding bands which determine the nearest neighbor bond strength. Indeed, as we have indicated in discussing our X-ray diffraction results, we might anticipate little change in nearest neighbor configuration accompanying the observed structural changes.

One consequence of the tentative association of the refractive index changes of evaporated As_2S_3 and As_2Se_3 with changes in E_o is that the first peak in ϵ_2 for the polymerized films must be sharper than for the more molecular films, inasmuch as the shifts of E_o are much larger than the shifts of the optical absorption edge. The largest edge shift we have

observed occurs for the case of illumination of evaporated As_2S_3, and is only ~0.06 eV, much smaller than the preliminary values for the shifts in E_o. For the reversible photodarkening of previously annealed As_2S_3 and As_2Se_3 films the absorption edge shifts are sufficiently small (0.03 eV for As_2S_3, which had the largest shift) that a comparable shift of the entire ϵ_2 spectrum of, say, 0.03 eV would not produce an observable change in refractive index ($\Delta n \leq 0.01$), assuming the dispersion relationship given in equation 4.

Analogies to the observed thermostructural and photostructural effects in evaporated As_2Se_3 films occur in the cases of white phosphorous and yellow arsenic[41], both large gap metastable crystals which can only be produced by the condensation of tetrahedral P_4 and As_4 molecules on chilled substrates, and which polymerize upon heating (and illumination, in the case of yellow arsenic[24]) to form the respective covalent network glasses[41]. Another analogy to the proposed photo and thermal polymerization is the transformation on heating to about 30°C of red amorphous Se[42] which presumably contains no Se_n chains, to black amorphous Se which contains substantial concentrations of both Se_n chains and Se_8 rings. The crystalline version of this latter reaction which also involves a shift of optical absorption to lower energies occurs when α or β monoclinic selenium containing only Se_8 rings rapidly transforms (or polymerizes) at ~150°C to hexagonal selenium which contains only Se_n chains[43].

The origin of the optical effect leading to photodarkening of the

annealed films remains unexplained. We tentatively associate this effect with a non-equilibrium excess of trapped holes and electrons which are incapable of reequilibrating at the temperature at which they are produced. Such trapped charges must lie within the mobility edges in sites which are sufficiently localized and deep-lying to inhibit recombination or reequilibration with thermally generated carriers. Presumably the electrostatic attraction of excess trapped charges constitutes a local deformation which could affect the joint density of lone-pair and conduction band states at energies approaching the optical gap energy.

To summarize these observations, we would like to distinguish between two modes of photo response of amorphous chalcogenide alloys. These modes, termed the photodarkening mode and the photostructural mode grade imperceptibly into one another. However, the photostructural mode is characterized by shifts of both optical absorption edge and refractive index upon illumination, leading to a perturbation of the W-D oscillator parameters, while the photodarkening mode is characterized by a shift of optical absorption edge unaccompanied by a significant change of refractive index or W-D oscillator parameters. For As_2S_3 and As_2Se_3, the local order, as given by the X-ray diffraction pattern, is strongly perturbed in the photostructural mode, and essentially unaffected in the photodarkening mode.

While we have only peripherally observed some of the photochemical effects which accompany illumination of these alloys, e.g., our observations on photo-enhanced oxidation of evaporated As_2S_3 layers in a poor vacuum which confirm the observations of Berkes et al.[5], the analysis of the photo response in terms of the photostructural mode and the photodarkening mode bears on these photochemical effects. A second photochemical effect which involves the diffusion of silver into evaporated As_2S_3 layers in the presence of band-gap illumination[9], can be viewed as a technique for development of the photostructural "images" in the pure chalcogenide layers. Some insights are provided by such photodoping on the structural state of evaporated As_2S_3 layers. For example, we have observed that photodoping does not involve the formation of crystalline Ag_2S which would be anticipated if the primary photo-event in the as-deposited film resulted in the formation of an S-rich phase as a consequence of phase separation. Both of these photo-enhanced chemical reactions (oxidation and Ag diffusion), which can be schematically represented:

$$(As_2S_3)_a + O_2 \xrightarrow{h\nu} (As_2O_3)_x + S_x$$

$$(Ag)_x + (As_2S_3)_a \xrightarrow{h\nu} (Ag, As, S)_a$$

where 'a' represents the amorphous and 'x' represents the crystalline phase, are thermodynamically favored at room temperature (as indicated, for example, by the fact that both reactions are accelerated at higher

temperatures) but are essentially inhibited by some kinetic barrier in the absence of band-gap illumination. Therefore the role of light and its photostructural concomitants can be viewed as that of a catalyst in lowering the activation barrier to a thermodynamically favored, though kinetically inhibited, chemical reaction. The As_2S_3 itself is not a true catalyst, of course, because it participates in both reactions, but its photo-enhanced reactivity might indicate enhanced catalytic activity with respect to some chemical reaction in which As_2S_3 cannot participate.

Since we consider that the photochemical activity of As_2S_3 is closely related to its photostructural activity, the atomistic picture of the two effects can be discussed in parallel as well. In describing the photo response of As_2S_3, we were concerned with two effects: photo-polymerization and non-equilibrium trapped holes and electrons. Both effects involve a perturbation of the equilibrium concentration of holes, trapped electrons, and broken bonds (uncharged free radicals). In the intermediate stages of polymerization an excess concentration of broken bonds may be required in order to effect the required reconstructive transformation. Catalytic effects in semiconductors are traditionally associated with the free carrier character at surfaces, and the role of illumination and impurities in enhancing this free carrier character is well documented[44]. In amorphous semiconductors the localized states which are associated with trapped carriers or broken bonds provide a possible source of

catalytic action, and may constitute the link between the photostructural transformations and the observed photochemical activity of As_2S_3 and related materials. We intend to examine the relationship between the structural state and the chemical reactivity of As_2S_3 in future experimental studies.

V. SUMMARY AND CONCLUSIONS

1. Slowly evaporated amorphous films of As_2S_3 and As_2S_3 undergo structural transformations when exposed to band gap illumination (photostructural transformation) or when annealed at $\sim T_g$ (thermostructural transformation).

2. The initial structures of these evaporated amorphous solids appear to retain the molecularity which characterizes the vapor from which they are condensed.

3. In the case of slowly evaporated As_2S_3, the X-ray diffraction pattern is well characterized in terms of a dense-random packing of As_4S_6 molecular "hard-spheres", and the density calculated from this structural model agrees well with the measured density.

4. X-ray patterns of the transformed evaporated As_2S_3 and As_2Se_3 films closely resemble patterns of the sputtered films and the bulk glasses, indicating that polymerization of the molecular units occurs during the photostructural and thermostructural transformations of the evaporated films.

5. The refractive indices of the evaporated films increase irreversibly with annealing at T_g or with band-gap illumination, attaining values close to the bulk glass value for As_2S_3. No measurable change ($\Delta n < 0.01$) of refractive index accompanies illumination of the annealed films or annealing of the illuminated films.

6. The optical absorption edge energy of the evaporated films decreases irreversibly with annealing at T_g or with band-gap illumination.

A decrease of absorption edge energy accompanies exposure of the annealed films, and the edge can be reversibly restored by reannealing. This shift, termed photodarkening, is small for As_2Se_3 (~0.01 eV) and somewhat larger for As_2S_3 (~0.03 eV).

7. The irreversible optical effects accompany the irreversible structural effects, and can be qualitatively associated with polymerization, by analogy with the optical properties of the sequence of selenium phases: monoclinic (Se_8 rings only)⟶ amorphous (Se_n chains plus Se_8 rings)⟶ hexagonal (Se_n chains only) for which the absorption edge energy decreases continuously and the refractive index increases continuously.

8. During long illuminations in high vacuum photo-induced evaporation of very thin films of As_2S_3 produces a mottled structure reminiscent of phase separation as observed by TEM. The homogenization of this mottling with mild electron-beam heating indicated that the mottling can be attributed to thickness fluctuations rather than to compositional fluctuations.

9. The optical effects in As_2Se_3 and As_2S_3 can be entirely accounted for in terms of defect formation (photodarkening) and polymerization (photostructural and thermostructural changes), and no optical evidence for phase separation was obtained. Conversely, the parallel shifts of the absorption edge accompanying illumination or annealing are inconsistent with the segregation of a

heavily absorbing second phase such as amorphous arsenic or with any change of light scattering which would accompnay phase separation.

10. The enhanced chemical reactivity of As_2S_3 accompanying exposure to band-gap illumination, such as oxidation in a 10^{-6} torr vacuum or reaction with a thin Ag underlayer, appears to be a concomitant of the photostructural transformation, possibly involving localized electronic defects including trapped charges and broken bonds.

VI. ACKNOWLEDGEMENTS

We acknowledge the support of the Advanced Research Projects Agency under Contract No. DAHC15-70-C-0187. In addition we thank H. Fritzsche for his unpublished mass spectrometer analysis of the As_2Se_3 vaporization products and for numerous discussions regarding the optical properties. The technical assistance of R. Goss, R. Seguin, J. E. Tyler, P. K. Flynn, T. Sebring and R. S. Nowicki is gratefully acknowledged. Mr. and Mrs. C. V. Pellier of Pellier-Delisle Metallurgical Laboratory constructed the model of the As_4S_6 molecule.

References

1. J. Feinleib, J. deNeufville, S. C. Moss and S. R. Ovshinsky, Appl. Phys. Letters 18 (1971) 254; see also R. J. von Gutfeld and P. Chaudhari, J. Appl. Phys. 43 (1972) 4688; K. Weiser, R. J. Gambino and J. A. Reingold, Appl. Phys. Letters 22 (1973) 48.
2. J. Feinleib, S. Iwasa, S. C. Moss, J. deNeufville and S. R. Ovshinsky, J. Non-Crystalline Solids 8-10 (1972) 909.
3. S. R. Ovshinsky and P. Klose, J. Non-Crystalline Solids 8-10 (1972) 892; see also S. R. Ovshinsky, Proc. Fifth Annual Natl. Conf. on Industrial Res. (1969) 68.
4. R. G. Brandes, F. P. Laming and A. D. Pearson, Applied Optics 9 (1970) 1712.
5. J. S. Berkes, S. W. Ing and W. J. Hillegas, J. Appl. Phys. 42 (1971) 4908.
6. S. A. Keneman, Appl. Phys. Letters 19 (1971) 205.
7. Y. Ohmachi and T. Igo, Appl. Phys. Letters 20 (1972) 506.
8. T. Igo and Y. Toyoshima, J. Non-Crystalline Solids 9 (1972) 139; ibid 11 (1973) 304.
9. H. Sakuma, I. Shimizu, H. Kokado and E. Inoue, Proc. 3rd Conference on Solid State Devices, Tokyo 1971; suppl. to Oyo Buturi 41 (1972) 76.
10. M. B. Myers and E. J. Felty, Mater. Res. Bull. 2 (1967) 535.
11. J. deNeufville, J. Non-Crystalline Solids 8-10 (1972) 85.
12. J. Schottmiller, M. Tabak, G. Lucovsky and A. Ward, J. Non-Crystalline Solids 4 (1970) 80.

13. S. Tsuchihashi and Y. Kawamoto, J. Non-Crystalline Solids 5 (1971) 286.

14. A. Renninger, Thesis for the ScD. Degree, Dept. of Metallurgy and Materials Science, M.I.T. Cambridge, Mass, June (1972).

15. M. Rubenstein and P. C. Taylor, Phys. Rev. Letters 29 (1972) 119.

16. G. Lucovsky, Phys. Rev. B 6 (1972) 1480.

17. A. D. Pearson and B. G. Bagley, Mater. Res. Bull. 6 (1971) 1041.

18. See, for example, M. L. Theye, Mater. Res. Bull 6 (1971) 103; H. K. Rockstad and J. deNeufville, Proc. XI Int'l Conf. on Physics of Semicond. (Warsaw, 1972) pp. 542 - 548.

19. M. Hansen, Constitution of Binary Alloys (McGraw-Hill, New York, 1958) p. 177.

20. J. W. Cahn and R. J.Charles, Phys. Chem. Glasses 6 (1965) 181.

21. G. C. Das, M. B. Bever, D. R. Uhlmann and S. C. Moss, J. Non-Crystalline Solids 7 (1972) 251.

22. E. A. Fagen, unpublished research.

23. B. C. Giessen and C. J. J. Wagner, in: Liquid Metals, S. Beer, ed. Marcel Dekker, New York, 1972) p. 633.

24. A. F. Wells, Structural Inorganic Chemistry, Oxford University Press, Oxford, 1962) p. 682.

25. H. Fritzsche, private communication.

26. G. S. Cargill III, J. Appl. Phys. 41 (1970) 2248; D. E. Polk, Acta Met. 20 (1972) 485; D. E. Polk, J. Non-Crystalline Solids 11 (1973) 381.

27. S. C. H. Lin and P. Duwez, Phys. Status Solidi 34 (1969) 469.

28. G. S. Cargill III, J. Appl. Phys. 41 (1970) 1.

29. J. L. Finney, Proc. Roy. Soc. (London) A319 (1970) 479.

30. A. K. Sinha and P. Duwez, J. Phys. Chem. Solids 32 (1971) 267.

31. R. E. Drews, R. L. Emerald, M. L. Slade and R. Zallen, Solid State Commun. 10 (1972) 293.

32. S. H. Wemple and M. DiDomenico, Jr., Phys. Rev. B 3 (1971) 1338.

33. S. H. Wemple, Phys. Rev. B 7 (1973) 3767.

34. R. K. Galkiewicz and J. Tauc, Solid State Commun. 10 (1972) 1261.

35. W. S. Rodney, I. H. Malitson and T. A. King, J. Opt. Soc. Am. 48 (1958) 633.

36. R. J. F. Dairymple and W. E. Spear, J. Phys. Chem. Solids 33 (1972) 1071.

37. J. Stuke, J. Non-Crystalline Solids 4 (1970) 1.

38. J. Schottmiller, M. Tabak, G. Lucovsky and A. Ward, J. Non-Crystalline Solids 4 (1970) 80.

39. W. G. Wyckoff, Crystal Structures (Interscience Publishers, New York, 1963).

40. R. Kaplow, T. A. Rowe and B. L. Averbach, Phys. Rev. 168 (1968) 1068.

41. H. Krebs, Fundamentals of Inorganic Chemistry (McGraw-Hill, London, 1968).

42. H. Gobrecht, G. Willers and D. Wobig, J. Phys. Chem. Solids 31 (1970) 2145.

43. G. B. Abdullayev, Y. G. Asadov and K. P. Mamedov, in: The Physics of Selenium and Tellurium, edited by W. Charles Cooper (Pergamon, Oxford, 1969) pp. 179 - 197.

44. G.-M. Schwab in: Semiconductor Surface Physics (University of Pennsylvania Press, Philadelphia, 1957) pp. 283 - 296.

Figure Captions

Fig. 1. X-ray diffraction profiles of 2.0μm As_2Se_3 films vapor-deposited over Corning 7059 plates. The radiation is CuKα (λ = 1.54Å).. (a) Sequence of diffraction runs on a film after deposition, followed by illumination under white light and a final anneal. (b) Reverse sequence to (a) in which the anneal was followed by a final illumination.

Fig. 2. X-ray (CuKα) diffractometer profiles of a 22.0μm film of As_2S_3 before and after annealing below the glass transition temperature ($T_g \cong 230^{\circ}C$).

Fig. 3. Thick film diffraction from As_2Se_3 reproducing, in greater detail, the first two results of Fig. 1(b).

Fig. 4. Diffractometer profiles of sputtered As_2Se_3 before and after annealing.

Fig. 5. Diffractometer profiles of polished bulk As-Se glasses demonstrating the composition dependence of the structure of slowly cooled material.

Fig. 6. TEM results on a 500Å film of As_2S_3 deposited in a 10^{-8} vacuum followed by in-situ illumination. (a) Evaporated, unexposed area

(b) Evaporated area followed by exposure to filtered white light. The scale of mottling is ~ 1200Å - 1500Å. (c) Electron-beam heating of the area in (b) showing bubbling in the electron dense regions.

Fig. 7. Electron diffraction pattern of the exposed area in Fig. 6(b).

Fig. 8. Absorption coefficient, α, versus photon energy in eV for evaporated and sputtered As_2S_3 and As_2Se_3. (a) Influence of exposure and annealing on evaporated As_2S_3; (b) Influence of exposure and annealing on evaporated As_2Se_3; (c) Influence of exposure and annealing on sputtered As_2Se_3.

Fig. 9. Thermally induced optical changes in evaporated As_2Se_3 monitored through the absorption of weak 6328Å He-Ne laser illumination. The reversible changes are given by the temperature dependent absorption. The irreversible parts are due to the structural annealing.

Fig. 10. X-ray diffraction and optical transmission monitoring of photo-darkening in an evaporated As_2Se_3 film. The X-ray parameter (I_1/I_2) is the ratio of the first diffuse peak to the first diffuse minimum (see Figs. 1-3). The illumination is with an incandescent source while the optical monitoring is with the He-Ne laser.

Fig. 11. Progressive optical (6328Å He-Ne laser) and thermal (5 min. at

105°C) cycling of evaporated As_2Se_3 to demonstrate reversible versus cumulative photo and thermal treatments.

Fig. 12. Three views of the As_4S_6 (As_4Se_6) molecule as determined by electron diffraction from the vapor phase (see ref. 24). The S atoms (darker balls) are indicated by lobes representing the non-bonding p-type lone-pair electrons.

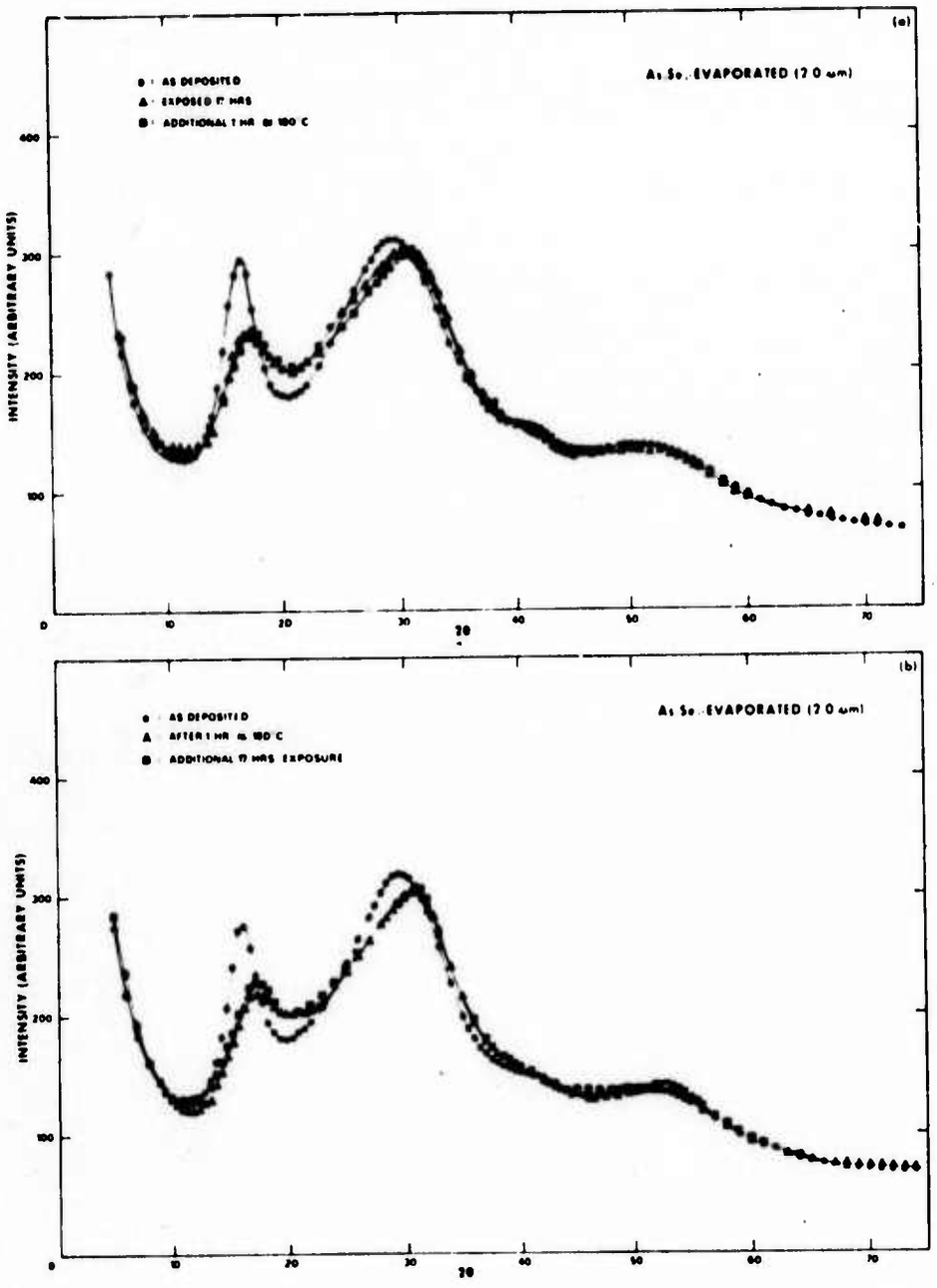
(a)
As Se EVAPORATED (7 0 μm)
AS DEPOSITED
EXPOSED 17 HRS
ADDITIONAL 1 HR @ 180 C
INTENSITY (ARBITRARY UNITS)
2θ
(b)
As Se EVAPORATED (7 0 μm)
AS DEPOSITED
AFTER 1 HR @ 180 C
ADDITIONAL 17 HRS EXPOSURE
INTENSITY (ARBITRARY UNITS)
2θ

Figure 1

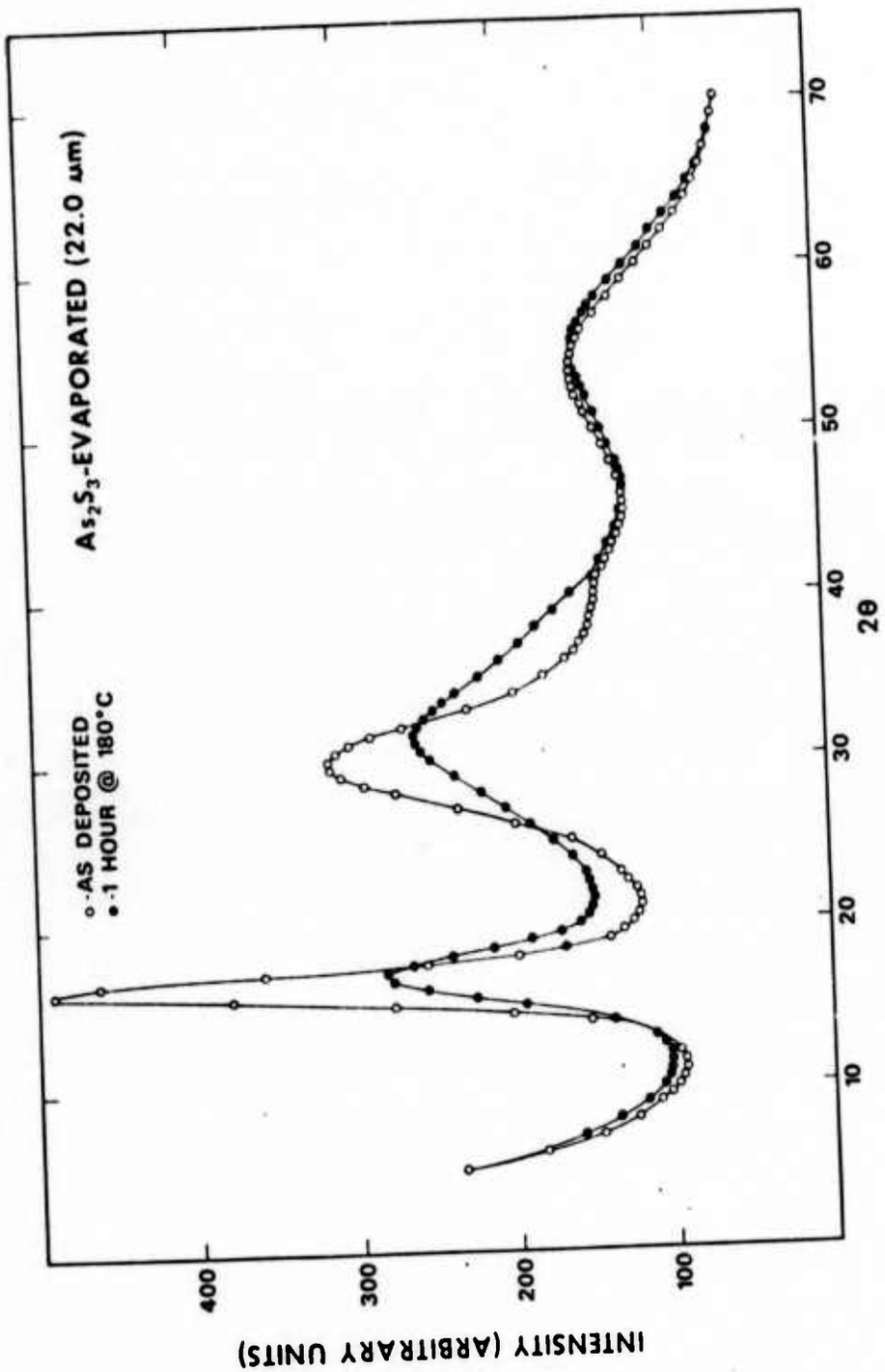
As_2S_3-EVAPORATED (22.0 μm)
○-AS DEPOSITED
●-1 HOUR @ 180°C
INTENSITY (ARBITRARY UNITS)
100
200
300
400
10
20
30
40
50
60
70
2θ

Figure 2

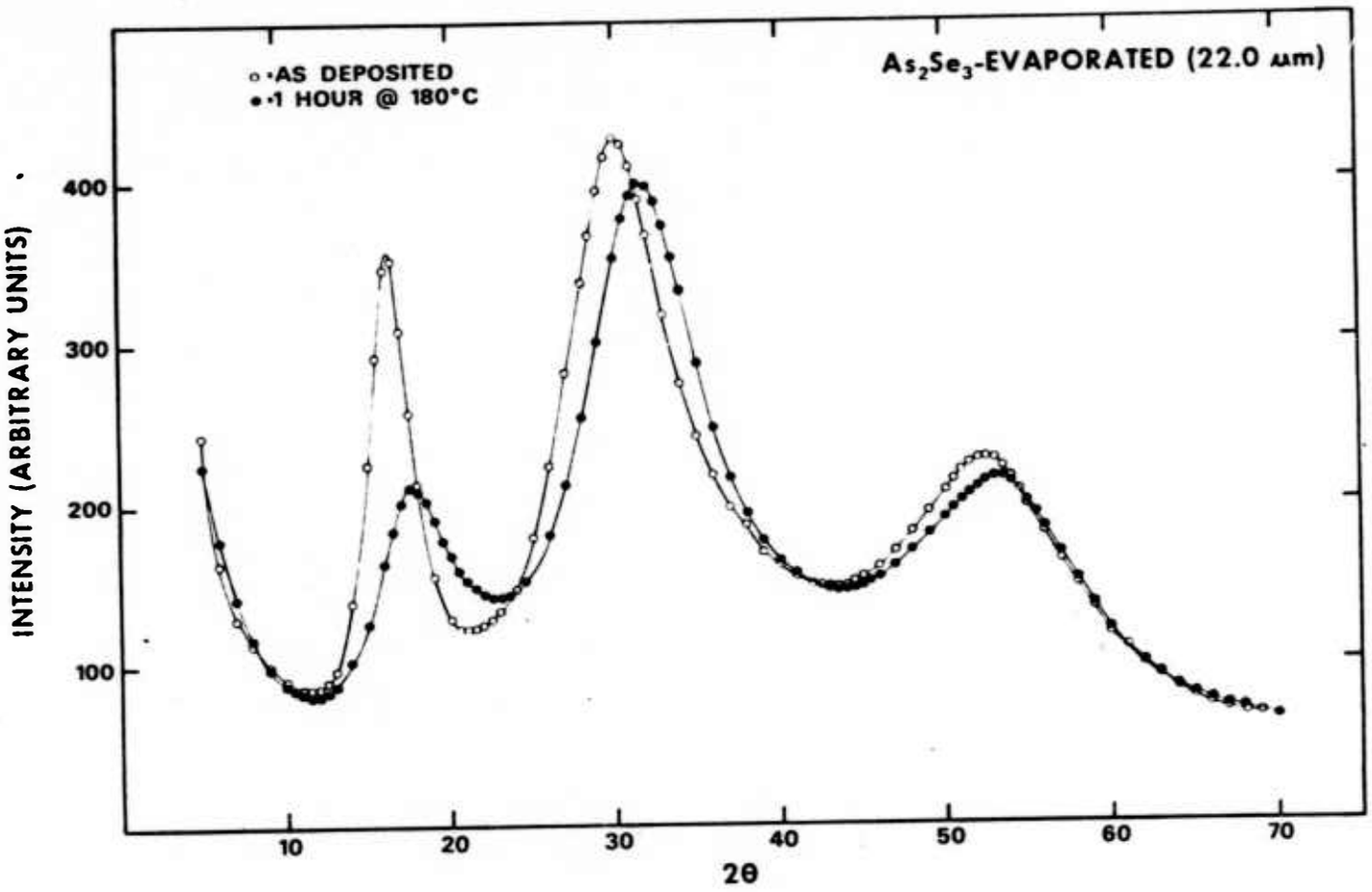
○ · AS DEPOSITED
● · 1 HOUR @ 180°C
As_2Se_3-EVAPORATED (22.0 μm)
INTENSITY (ARBITRARY UNITS)
400
300
200
100
10
20
30
40
50
60
70
2θ

Figure 3

As_2Se_3-SPUTTERED (10.9 μm)
○: AS DEPOSITED
●: 1 HOUR @ 180°C
INTENSITY (ARBITRARY UNITS)
100
200
300
400
10
20
30
40
50
60
2θ

Figure 4

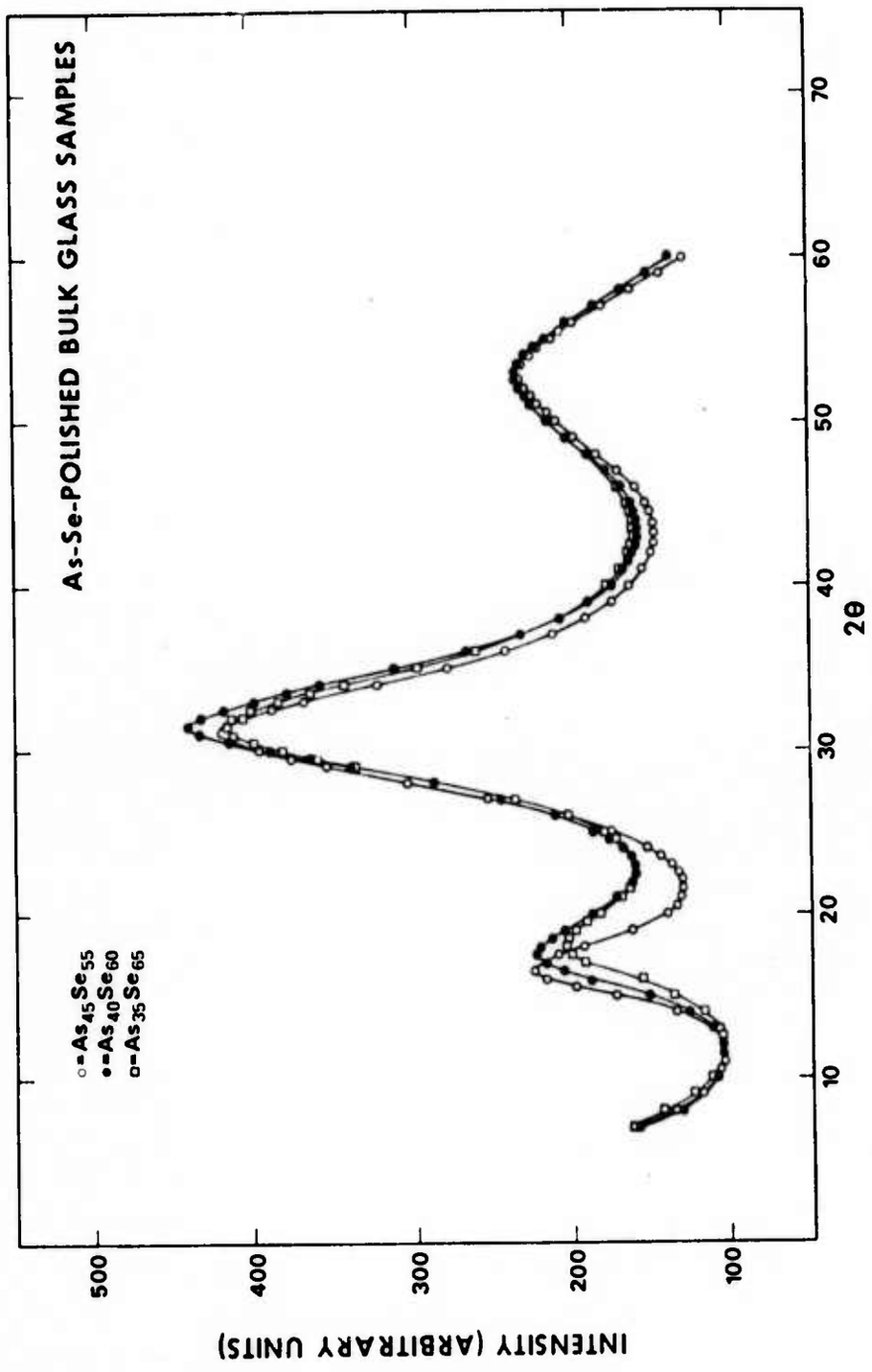
As-Se-POLISHED BULK GLASS SAMPLES
○=As45Se55
●=As40Se60
□=As35Se65
INTENSITY (ARBITRARY UNITS)
2θ
100
200
300
400
500
10
20
30
40
50
60
70

Figure 5

A

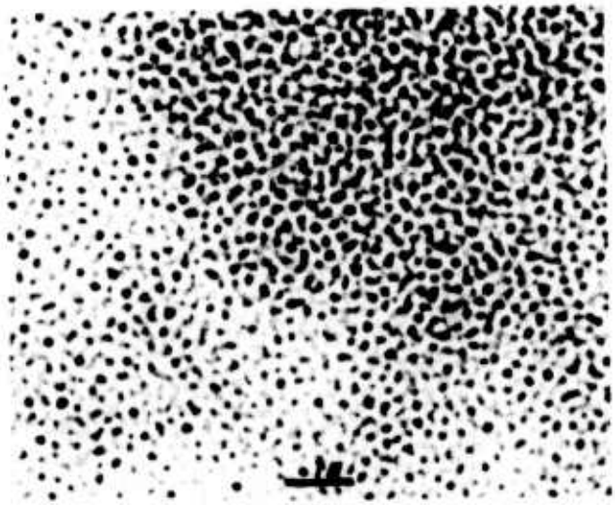

B

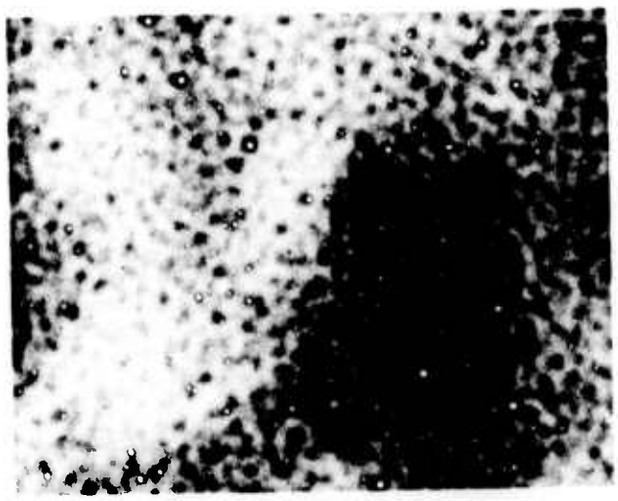

C

Figure 6

Figure 7

Figure 8

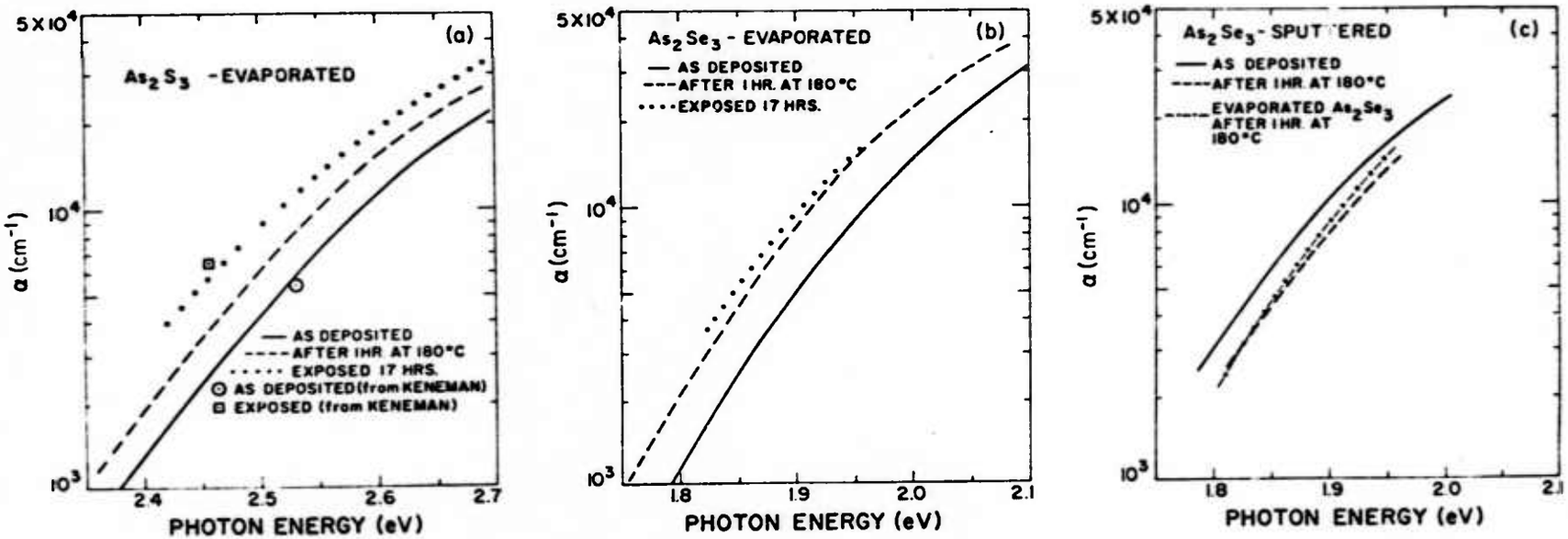
(a)
As2S3 -EVAPORATED
AS DEPOSITED
AFTER 1HR. AT 180°C
EXPOSED 17 HRS.
AS DEPOSITED (from KENEMAN)
EXPOSED (from KENEMAN)
α (cm⁻¹)
PHOTON ENERGY (eV)
(b)
As2Se3 - EVAPORATED
AS DEPOSITED
AFTER 1 HR. AT 180°C
EXPOSED 17 HRS.
α (cm⁻¹)
PHOTON ENERGY (eV)
(c)
As2Se3 - SPUTTERED
AS DEPOSITED
AFTER 1HR. AT 180°C
EVAPORATED As2Se3 AFTER 1 HR. AT 180°C
α (cm⁻¹)
PHOTON ENERGY (eV)

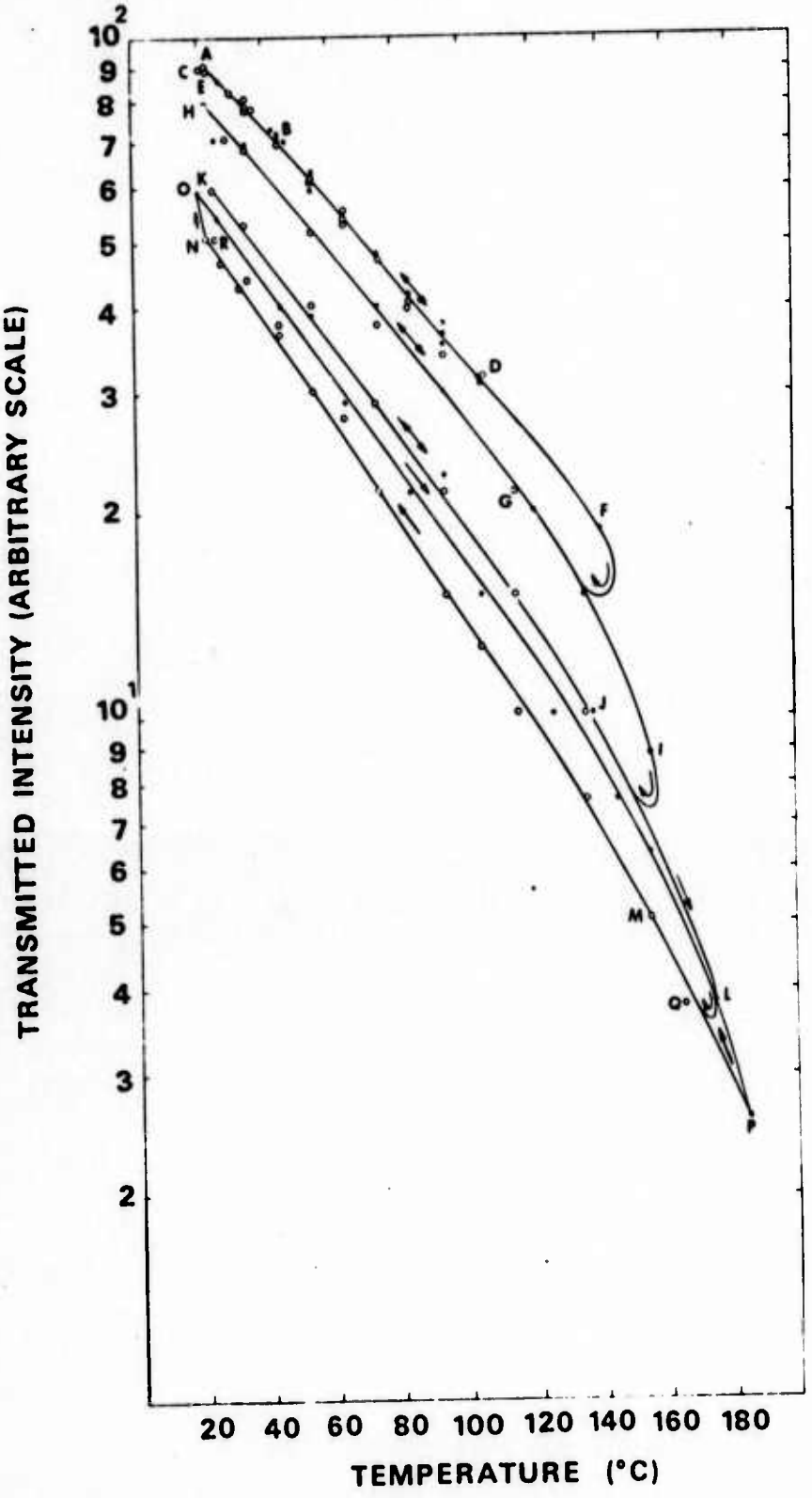
TRANSMITTED INTENSITY (ARBITRARY SCALE)
10^2
9
8
7
6
5
4
3
2
10^1
9
8
7
6
5
4
3
2
A
B
C
D
E
F
G
H
I
J
K
L
M
N
O
P
20 40 60 80 100 120 140 160 180
TEMPERATURE (°C)

Figure 9

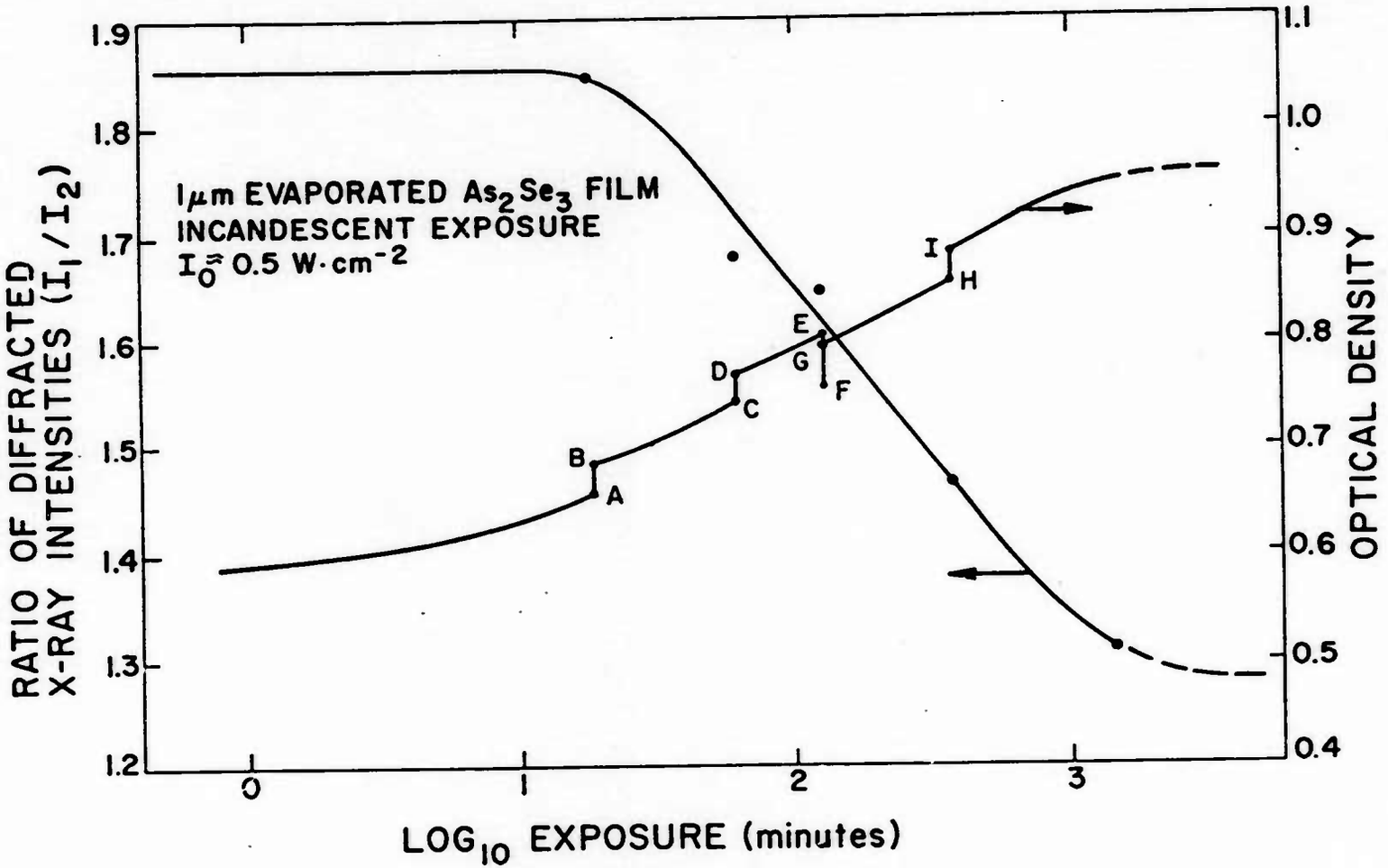
1μm EVAPORATED As_2Se_3 FILM
INCANDESCENT EXPOSURE
$I_0 \cong 0.5$ W·cm^{-2}
RATIO OF DIFFRACTED X-RAY INTENSITIES (I_1/I_2)
OPTICAL DENSITY
LOG_{10} EXPOSURE (minutes)
1.9
1.8
1.7
1.6
1.5
1.4
1.3
1.2
1.1
1.0
0.9
0.8
0.7
0.6
0.5
0.4
0
1
2
3
A
B
C
D
E
F
G
H
I

Figure 10

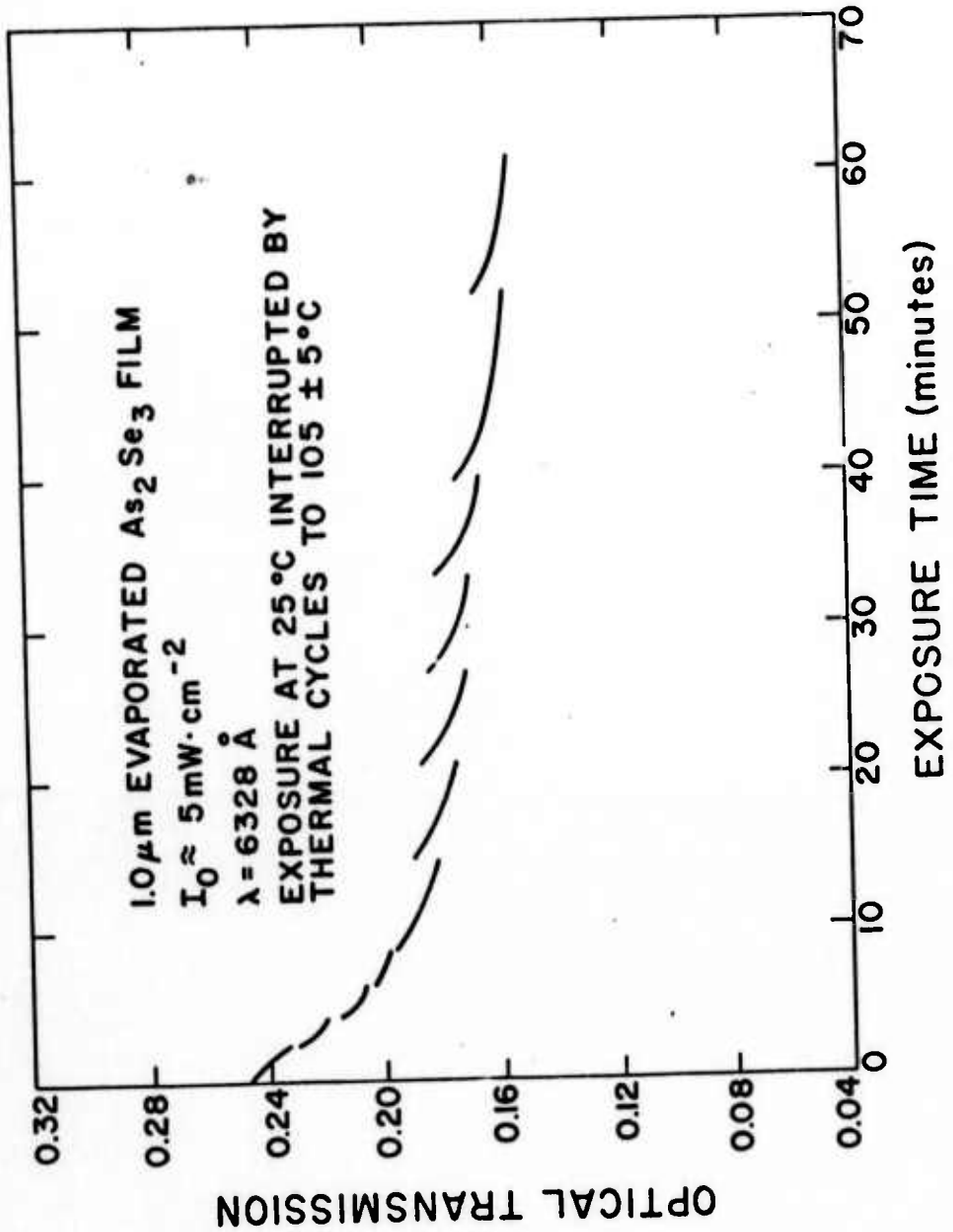
1.0μm EVAPORATED As_2Se_3 FILM
$I_0 \approx 5mW \cdot cm^{-2}$
λ = 6328 Å
EXPOSURE AT 25°C INTERRUPTED BY THERMAL CYCLES TO 105 ± 5°C
OPTICAL TRANSMISSION
0.32
0.28
0.24
0.20
0.16
0.12
0.08
0.04
0
10
20
30
40
50
60
70
EXPOSURE TIME (minutes)

Figure 11

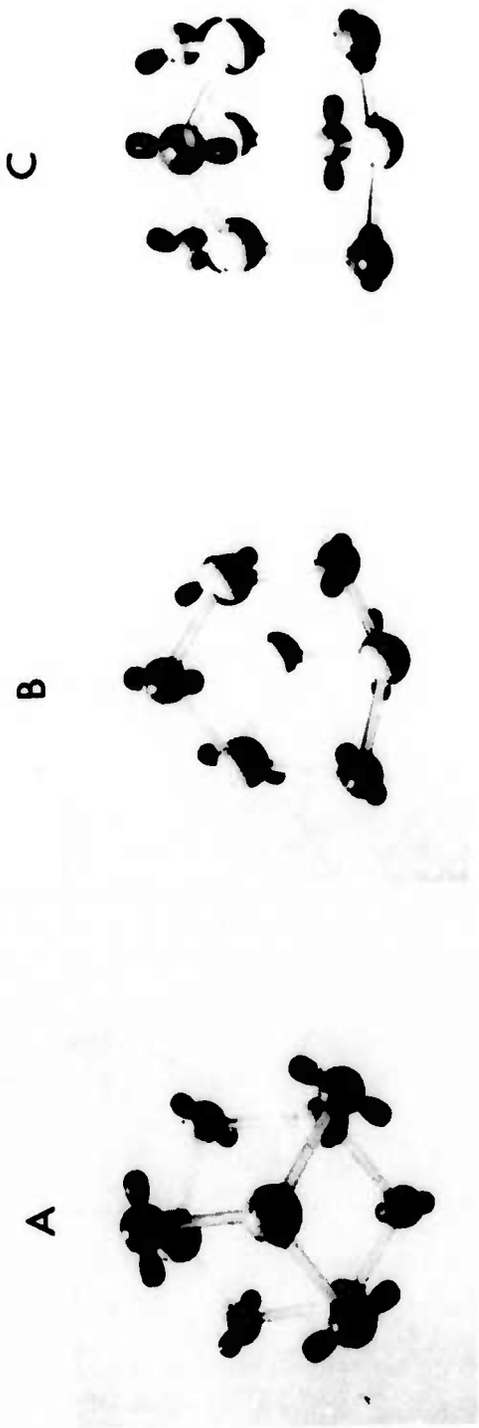

Figure 12